

Multipath mitigation of carrier-phase GPS position estimates from the Helheim glacier: using new reduced sidereal filtering approach

Master's Thesis in Radio and Space Science

JOHAN NILSSON

Department of Earth and Space Sciences
Division of Space Geodesy and Geodynamics
CHALMERS UNIVERSITY OF TECHNOLOGY
Gothenburg, Sweden 2011
Master's Thesis 2011:08

MASTER'S THESIS 2011:08

Multipath mitigation of carrier-phase GPS position estimates from
the Helheim glacier: using new reduced sidereal filtering approach

Master's Thesis in Radio and Space Science
JOHAN NILSSON

Department of Earth and Space Sciences
Division of Space Geodesy and Geodynamics
CHALMERS UNIVERSITY OF TECHNOLOGY

Gothenburg, Sweden 2011

Multipath mitigation of carrier-phase GPS position estimates from the Helheim glacier:
using new reduced sidereal filtering approach
JOHAN NILSSON

©JOHAN NILSSON, 2011

Master's Thesis 2011:08
ISSN 1652-8557
Department of Earth and Space Sciences
Division of Space Geodesy and Geodynamics

Chalmers University of Technology
SE-412 96 Gothenburg
Sweden
Telephone: + 46 (0)31-772 1000

Cover:
Original time-series filtered with ordinary sidereal filter and the reduced sidereal filter.

Chalmers Reproservice
Gothenburg, Sweden 2011

Multipath mitigation of carrier-phase GPS position estimates from the Helheim glacier:
using new reduced sidereal filtering approach
Master's Thesis in Radio and Space Science
JOHAN NILSSON
Department of Earth and Space Sciences
Division of Space Geodesy and Geodynamics
Chalmers University of Technology

Abstract

The Greenland ice sheet contains a vast volume of water frozen over millennia, which have in recent decades come under investigation, motivated by the possible effects of global warming. Recent observations have shown that outlet glaciers on the edges of Greenland's ice sheet is melting (retracting) at a unexpected rate, not perviously seen. So it is of vital importance that we understand the dynamics of the outlet glaciers on Greenland, such as Helheim, because they play a crucial part in the predictions of sea-level rise. Because resent investigations have seen an increase in glacier speed, calving rates, and glacial earthquakes. From this it is clear that the understanding of the dynamics and the link between these events are still poorly understood.

On the Helheim glacier we know that glacial earthquakes, calving and glacier speed up all happen close in time with respect to each other, but due to the multitude of noise and other signals, the specific earthquake time is hard to resolve. Sidereal filtering is an effective way to remove and reduce noise (which consists mostly of multipath) which has periodic behavior that repeats itself from day to day in the position estimates for high rate GPS. This technique has been uses primarily for earthquake deformation studies where the sites involved have been assumed to be stationary relative to each other before the earthquake. But in an environment of an outlet glacier like Helheim on Greenland this generalization does not hold. There is not only large motions in the flow of ice (~ 30 m/day), there are also significant tidal and diurnal motions associated with insolation and hydrology.

The purpose of this thesis is to extended the sidereal filtering approach to a glacial environment with the goal to remove high levels of noise. At the same time the goal is to preserve the dynamics of interesting periodic signals inherent in the data which are usually removed by the regular sidereal filtering.

I found that it is possible to extend the sidereal filtering technique to this kind of a highly variable environment. And that it's also possible to preserve the dynamics of periodic signals using this technique.

When applying this new extended technique preserving periodic behavior (reduced sidereal filtering) a reduction in noise in the range of 30 – 70 %, a signal degradation of 18 – 20 % and a reduction in variability of 4 – 20 %. For the ordinary sidereal filtering we found a noise reduction range of 45 – 90 % and signal degradation of 75 – 100 % and a reduction in variability between –28 – 85 %. Further I also found that correlation is a good overall description for repeatability and filter performance of the sidereal filtering technique in this environment. I also discovered that the reduction in noise for the reduced sidereal filter also strongly depends of the stations velocity profile.

Keywords: sidereal filtering, repeatability, correlation, multipath noise, noise reduction, signal degradation.

Contents

Abstract	I
Contents	III
Preface	V
1 Introduction	1
1.1 Purpose	2
1.2 Limitations	2
1.3 Approach	3
2 Global Positioning System	3
2.1 Introduction	3
2.2 Signal Structure	4
2.3 GPS Observables	6
2.3.1 Pseudo-range Observable	6
2.3.2 Carrier-Phase Observable	7
2.4 Single Differencing	8
2.5 Double Differencing	8
2.6 Error Sources	9
2.6.1 Relativistic effects	9
2.6.2 Satellite Clock Errors	9
2.6.3 Satellite Orbital Errors	10
2.6.4 Multipath Effects	10
2.6.5 Ionospheric Effects	11
2.6.6 Tropospheric Effect	11
2.6.7 Satellite Geometry	12
2.6.8 Receiver Noise and Clock Error	13
2.7 Geophysical Model and Reference System	13
2.8 Point Positioning using Pseudo-range	14
2.9 Relative Positioning using carrier phase	15
2.9.1 Kinematic relative position	16
2.10 Linear dependence of observations	16
3 Time Series Analysis	16
3.1 Statistical Analysis	17
3.1.1 Arithmetic Mean	17
3.1.2 Variance and Standard Deviation	17
3.1.3 Root Mean Square (RMS)	18
3.1.4 Correlation	18
3.1.5 Linear Regression and Residuals	18
3.1.6 Histogram	20
3.2 Spectral Analysis	20
3.2.1 Power Spectral Density	20
3.2.2 Integrated Power	21
3.2.3 Trapezoidal Numerical Integration	22
3.2.4 Noise and Signal Power Estimation	22

4	Time Domain Filtering	23
4.1	Sidereal Filtering	23
4.2	Reduced Sidereal Filtering	24
5	Frequency Domain Filtering	25
5.1	IIR Filter Design	25
5.1.1	Notch Filter Design by Pole-Zero Placement	25
5.1.2	Analog to Digital Conversion	26
5.2	IIR Filter Realization	26
5.2.1	Direct Form I	27
5.2.2	Direct Form II	27
5.3	Filter Stability	28
6	Variance Propagation and Reduction Models	28
6.1	Sidereal Filter Model	28
6.2	Reduced Sidereal Filter Model	29
7	GRASP Software Description	31
8	Data Processing and Methodology	33
8.1	Processing Strategy	33
8.2	Implementation & Parameter Estimation of Sidereal Filter	35
8.3	Implementation & Parameter Estimation of Digital Filter	36
9	Results	39
9.1	Filter Performance	39
9.2	Validation of Model	47
10	Discussion	48
11	Conclusion	49
12	Future Work	49

Preface

The idea of this thesis was born in the second year of the authors master program where he attended a course in satellite positioning held at Chalmers University of technology in Gothenburg, Sweden by Dr. Jan Johansson. In this course the author got a chance to write a thesis abroad due to the longstanding collaboration between Dr. Jan Johansson and Dr. James L. Davis at Onsala Space Observatory and Lamont-Doherty Earth Observatory.

Dr. James L. Davis needed someone to develop a graphical user interface for GPS data editing and a way to reduce noise in single-frequency carrier-phase measurements from there sites on Helheim glacier on Greenland. So the main objective of the thesis was to develop these two objectives from given specifications stated by Prof. James L. Davis.

The main work of the thesis was performed at Lamont-Doherty Earth Observatory and at Chalmers University of Technology during the period of January to September of 2011 under the supervision of Prof. James L. Davis.

Acknowledgments

I would like to thank Prof. James L. Davis for his great patience and his help with answering all the authors questions about programing and in the field of satellite geodesy. This has greatly helped the author during his time at Lamont. I would also like to thank Prof. Meredith Nettles for all her input on my graphical user interface and for always taking the time to help me with my project. Further I also would like to thank Prof. Jan Johansson for giving me this great chance and opportunity to write my thesis abroad in the United States. Last but not least I would like to thank my parents for there unwavering support of there son.

Gothenburg August 2011
Johan Nilsson

1 Introduction

The Greenland ice sheet contains a vast volume of water frozen over millennia, which have in recent decades come under investigation, motivated by the possible effects of global warming. Recent observations have shown that outlet glaciers on the edges of Greenland's ice sheet is melting (retracting) at a unexpected rate, not previously seen. So it is of vital importance that we understand the dynamics of the outlet glaciers on Greenland, such as the Helheim glacier, because they play a crucial part in the predictions of sea-level rise.

Recent investigations show short-time scale variations in glacier flow speed, a increasing number of glacial earthquakes and increased calving rates at Greenland's outlet glaciers. This suggests that the dynamics behind these events are still poorly understood. So in 2007 an investigation was launched at Helheim glacier (Greenland's third largest and most glacial earthquake intense outlet glacier) to better understand the connection between glacier speed, calving front behavior, and glacial earthquakes [5].

In this cross disciplinary experiment a network of twelve GPS receivers where continuously operating on the Helheim glacier to recored glacier flow speed, and other dynamics inherent to the glacier. Other sensors where also used, such as water pressure gauges, a broad band seismometer, and satellite imagery. In order to record calving front behavior, glacial earthquakes, and to measure the position of the calving front.

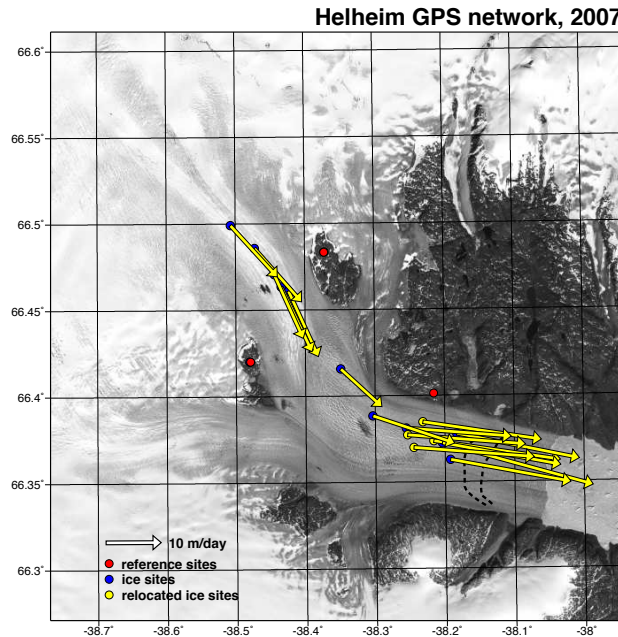


Figure 1.1: Network of GPS stations on the Helheim glacier, where yellow vectors indicate average GPS station velocity, red dots are rock-based reference stations and black dotted lines shows the position of the calving front of the years 2001 and 2007. (Courtesy of M. Nettles at Lamont-Doherty Earth Observatory of Columbia University)

On the Helheim glacier we know that glacial earthquakes, calving and glacier speed up, all happen close in time with respect to each other, but due to the multitude of noise and other signals (periodic and non-periodic) the specific earthquake time is hard to resolve. This makes it hard to distinguish between what causes what, thus the only thing that can be said is that they occur close in time to each other.

Sidereal filtering is an effective way to remove and reduce noise (mostly multipath) which have periodic behavior that repeats itself from day to day in the position estimates

for high rate GPS. So extending the sidereal filtering technique to glacial environments would be very useful in the sense that multiple signals and high noise levels makes accurate timing difficult.

This technique has been used primarily for earthquake deformation studies where the sites used have been assumed to be stationary with respect to each other before the earthquake. However in an environment of an outlet glacier like Helheim this generalization does not hold. There is not only large motions in the flow of ice (~ 30 meter per day), there are also significant tidal and diurnal motions associated with insolation and hydrology affecting the position estimates. What makes sidereal filtering so effective in reducing noise also gives it an inherent draw back. This approach is not only good at reducing noise, it is also good at reducing all other common mode signals in the data (mostly periodic). This poses a problem for the glacial environment which contains a lot of periodic (repeating) signals that are of interest for the investigation.

Writing GPS processing software that can detect and remove outliers and cycle slips is in general not easy. If for example a outlier detection script is too harsh it can reduce and remove the dynamic structures in the data. Further cycle slips are not always perfect integers or they may also be real jumps in the data misinterpreted by the cycle slip detector. So the best detector is still the human brain which can intelligently and rationally interpret data. Therefore in order to visually determine what is an outlier or a cycle slip there is a need to build software packages that can give the user the opportunity to easily browse through and edit large data sets.

1.1 Purpose

The goal of this thesis is first to investigate if it is possible to extend the sidereal filtering technique to a highly dynamic and kinetic environment such as an outlet glacier. But also to go a step further and try to preserve the dynamics of the periodic signals in the geodetic time-series, usually filtered away by the regular sidereal filtering. We will characterize the filter performance by:

- modeling the reduction of the standard deviation (RMS) to determine governing parameters.
- reduction of multipath noise.
- degradation of geodetic signals.

The second goal of this thesis is to develop a graphical user interface in MATLAB for GPS data editing, called GRASP (GPS residual Analysis Program). The purpose is to help the user to detect and remove outliers and cycle slips from the position estimate residuals from BAKAR, see chapter 7. A program developed for GPS kinematic positioning of single-frequency carrier-phase GPS data, written by James. L. Davis and Pedro. Elosegui.

1.2 Limitations

This study will be limited to the dual frequency position estimates from one specific site on Helheim glacier, which are converted into along flow position, see [5]. Data were collected with a 15 s sampling interval in 2007 from (GPS-days) 186 – 205 (21 day time series). The baseline was formed using kinematic relative positioning, see [5], using the IS22 site (based on the glacier) which was differenced against a rock bases reference station. Ionospheric and other baseline-related effects are assumed to be negligible due to short baseline, less than 30 km [3].

For this investigation only one sidereal time shift was considered when designing the sidereal filter.

1.3 Approach

The outline of this thesis can be divided up into two parts. Part one includes software and processing script development and part two entails using and applying the developed scripts and software on geodetic time-series and analyzing the results.

The initial and first step of this thesis is going to be the design of the graphical user interface in MATLAB, called GRASP. When this is achieved scripts and functions in MATLAB will be written to make it possible to implement the sidereal reduced sidereal filter to geodetic time-series.

The approach to extend the sidereal filter (SDF) to form the reduced sidereal filter (RSDF). This will be done in the following manner: First the data sets will be de-trended to remove all rates ($\sim 20 - 30$ per day). After this is done the sidereal filter will be constructed from two consecutive days of data, with a specific sidereal time shift. Then a digital filter will be designed to remove specific frequency bands in the sidereal filter. The digital filter is then applied to the sidereal filter. And this filtered sidereal filter (reduced sidereal filter) is then applied to the original data.

To estimate and predict filter performance models for both the SDF and RSDF are developed to determine the reduction in RMS. Then the reduction model will be compared with the observed reduction in RMS, this to validate and help characterize filter performance.

Then the observed results from the RSDF-approach and SDF-approach will be analyzed to determine the effects on noise reduction, signal degradation and reduction in the RMS of the time series.

2 Global Positioning System

2.1 Introduction

GPS started to be developed in the late 1960 by the US Department of Defense in collaboration with the US Navy and Air Force and was approved in 1973. The first satellite was launched in 1978 and the GPS system was considered operational in 1994.

The GPS system consists of a satellite constellation of 24+ satellites in Medium Earth Orbit (MEO) around the Earth, at an altitude of 20 000 m, an inclination of 55 degrees and a orbital period of 12 hours. The satellite constellation is divided into six orbital planes with a maximum of four satellites in every plane. The satellite constellation is configured so there always will be four satellites above the horizon at an elevation angle of at least 5 degrees which will give a total real time coverage of 99.9 %

The fundamental navigation principle is to measure what is called pseudo-ranges, between the user and the GPS satellites. To be able to solve for the coordinates of an receiver there must be at least four satellites above the horizon to triangulate the position. Using the coordinate reference frame called WGS 84 and known satellite coordinates the user position on the earth can be determined. The GPS satellites broadcast two carrier frequencies in the L-band ($L1 = 1575.42$ MHz and $L2 = 1227.60$ MHz). Modulated on these two frequencies are the navigation signals and navigation and system data. The signals are modulated with the so called pseudo-random noise sequence or the PRN where the navigations signals are separated into two codes (signals), the P-code and C/A-code. The

P-code is more precise than is the C/A code and are modulated on both frequencies instead of the C/A code which is only modulated on the L1 frequency. GPS satellites can be distinguished by their PRN carriers, every satellite has its own unique PRN number, between 1 – 37. Each satellite has four atomic clocks to be able to keep the high frequency standards that are needed to have a precise time base, with an accuracy of $1 \cdot 10^{-12}$ to $1 \cdot 10^{-13}$ [1].

The life time for GPS satellites are set by the U.S. Air Force to be around 6 – 10 years. The satellites are controlled by the control segment which task is to monitor the GPS system, determine the satellites trajectories, and clock parameters, upload data to satellites and if needed to do orbital maneuvers. This is done by five ground stations spread evenly around the equator that are in 24 h contact with the satellites that are above the station’s horizon. The data are then linked to the main facility in Colorado Springs, USA. Where all the orbital and clock parameters are solved and predicted for the near future and then uploaded again to the satellites. These updates have the function of synchronizing the atomic clocks within a few nanoseconds on every satellite and to adjust the internal orbital model of each satellite.

2.2 Signal Structure

There are two types of signals transmitted from the GPS system, the C/A-code (Coarse/Acquisition) and the P-code (Precision). The P-code is not transmitted, instead its cross-correlated with an encryption code W and becomes the Y code. It’s the Y-code that is transmitted from the satellite, this is called the P(Y)-code. The P(Y) code is not available for civilian users. Its open only for the US military and it’s allies. For civilian users only the C/A code is available and used for positioning.

Table 2.1: GPS carrier frequencies, where 10.23 MHz is the fundamental frequency of the atomic clocks [1]

L1 = 1575.42 MHz	154×10.23 MHz
L2 = 1227.6 MHz	120×10.23 MHz

The receiver can distinguish between the different signals from the satellites because GPS uses code division multiple access (CDMA) techniques where a low bit rate message is encoded with with a high rate pseudo random sequence (PRN) that is different for every satellite. The PRN is generated from 1-37 where 1-32 are the different and unique codes for every satellite and the rest are reserved for ground transmission.

The P-code is generated at a rate of 10.23 Mb/s and each satellite is assigned a portion of this code. The portion of this code repeats itself every 7 days and the total code is 37 weeks long, after 37 weeks it is renewed. All satellites transmit there own portion of the P-code on the two same frequencies this means that the receiver has to identify each satellite. This is solved by, as said before, assigning each satellite with its own particular week of the 37 week code. The receiver now knows which satellite has the different week and can recognize it by the navigation message and the particular GPS week which has to be very accurate, but this is usually found in the C/A code.

The C/A code is generated with a rate of 1.023 Mb/s, thus 10 times slower then the P-code, but the identification of the C/A-code is much simpler than the P-code and easier to acquire due to that it repeats every millisecond. Every satellite broadcasts its own unique PRN code which is 1023 bits long and which repeats every millisecond.

The GPS navigation message is transmitted at a frequency of 50 Hz and contains a master frame of 25 frames, each frame is 1500 bits long and divided into five subframes, which are comprised of 10 words. Each word is 30 bits long which makes the whole navigation message 37500 bits long and at a bit rate of 50 bps it takes 12.5 min to transmit and receive.

Table 2.2: GPS-codes [1]

Parameters	C/A-code	P-code	Navigation Message
Code rate	1.023 Mb/s	10.23 Mb/s	50bps
Code length	≈ 300 m	≈ 30 m	≈ 6000 m
Repetition	1 ms	1 week	N/A
Code type	37 unique codes	37 unique week segments	N/A
Properties	easy to acquire	more accurate	time ephemeris

Below is the full signal structure of the GPS-satellite signal, where $P(t)$ is the P-code, $C(t)$ is the C/A code, $W(t)$ is the encryption code and $D(t)$ is the navigational message, modulated on the two carrier frequencies $L1$ and $L2$ [1].

$$L_1(t) = a_1 P(t)W(t)D(t)\cos(f_1 t) + a_1 C(t)D(t)\sin(f_1 t) \quad (2.1)$$

$$L_2(t) = a_2 P(t)W(t)D(t)\cos(f_2 t) \quad (2.2)$$

The navigation message contains five subframes that all contains different information. Information in subframe 1 – 3 never change but 4 – 5 does. Subframes 1 – 3 contains all the information about the satellite such as clock corrections, orbit parameters and such. Subframes 4 – 5 contain atmospheric corrections for troposphere and ionosphere. The satellite almanac contains all the information about the other satellites in orbit and their navigation messages.

To be able to calculate the position of the user the receiver acquire and track the satellites using their C/A and P-codes (using their unique PNR code). To do this the receiver generates its own copy of the codes for the different PRN's internally and then uses the auto correlation to find and lock on to the satellites that are currently available over the horizon.

When the receiver finds that full correlation is achieved the receiver locks on to the signal and starts to measure the time delay between the received and generated code segment. The code is time stamped when it leaves the satellite with the satellite clocks own time. Then the difference is compared to the receivers clock, which makes it possible to find the pseudo-range.

Table 2.3: GPS satellites transmitted codes and carriers

Category	Observable
Carrier	$L1, L2$
Codes	$P1, P2, C1$ and $C2$

2.3 GPS Observables

GPS positioning is based on a very simple relation which is used in every day life. To find the position we only need to calculate the distance (slant range) between the receiver and the satellite and use several satellites to triangulate the position. Distance from the satellite is calculated using the simple relation:

$$\text{Distance} = \text{speed of light} \cdot \text{travel time}$$

This is a simple assumption and in real life we will have to correct for propagation delays of the signal due to the atmosphere, orbits and geometry. These will be further explained and introduced in the following sections.

The pseudo-range and carrier-phase observables will now be presented.

2.3.1 Pseudo-range Observable

Pseudo range measurement is described by the following simplified model where the observation to satellite S can be written as [3]:

$$P^S = (T - T^s)c \quad (2.3)$$

where t is the time in the receiver and T is the satellite transmission time and c is the speed of light in vacuum. This is not the true measure of distance, to model the true distance in the simplified case we have to take into account errors in accuracy both in the receiver clock and in the satellite clock.

$$T = \tau + dt \quad (2.4)$$

$$T^s = \tau^s + dt^s \quad (2.5)$$

where τ is the true time and dt is the introduced clock bias for both the receiver and the satellite clock. Now substitution gives the pseudo-range as a function of true time and clock bias.

$$P(t)^S = \rho(t, t^S)^S + c(dt - dt^s) \quad (2.6)$$

where $\rho(t, t^S)^S$ is, the true distance/range from the receiver at the specific epoch t compared to the satellites transmit time. To compute ρ we can use basic geometry and calculate the euclidian distance using a known satellite position in cartesian coordinates (x, y, z) in an Earth centered reference system. Excluding all other propagation errors and the uncertainty in the satellite orbit coordinates. We get the following relation [3]:

$$\rho^S = \sqrt{(x - x^S)^2 + (y - y^S)^2 + (z - z^S)^2} \quad (2.7)$$

Here the time dependence have been excluded for easier notation. This system contains four unknowns (x, y, z, τ) . This means that we have to use four satellites to solve the system of equations.

Before we have only taken into account clock bias in the model now we have to expand it to contain atmospheric propagation delays and observational noise. This is done by introducing delays due to the troposphere Z , ionosphere I errors due to multipath ε_m and receiver noise ε_p .

$$P(t)^S = \rho(t, t^S)^S + c(dt - dt^s) + I + Z + \varepsilon_p + \varepsilon_m \quad (2.8)$$

Now we want to generalize the notation to be able to handle multiple satellites and receivers. This is done by introducing the subscript k and j , where k is the receiver and j is the satellite, excluding the time dependence we get the following final expression for the pseudo-range:

$$P_k^j = \rho_k^j + c(dt_k - dt^j) + I_k^j + Z_k^j + \varepsilon_p + \varepsilon_m \quad (2.9)$$

2.3.2 Carrier-Phase Observable

Carrier phase measurements is when we use the carrier phase of the signal to measure the range. This is done by measuring the number of received cycles received by the receiver from the satellite. The measurement relation is based on the difference in phase cycles generated by the replica in the receiver and the actual received number of cycles from the satellite. This difference is usually called the carrier beat phase or just carrier phase [3].

$$\phi_B = \phi_{replica} - \phi_{signal} \quad (2.10)$$

This model is not fully complete because we can always add a arbitrary (integer) number of cycles to the carrier beat phase and construct exactly the same signal. Thus we can construct the following relation to describe the received phase [3]:

$$\Phi + N = \phi_{replica} - \phi_{signal} \quad (2.11)$$

where Φ is the recorded actual phase and N is the number of added integers. N is usually called the phase ambiguity and is an unknown constant that have to be solved for. If the receiver should lose count of the number phase changes we have what is called a cycle slip, which is similar to the phase ambiguity. However a cycle slip is not a constant for all measurements. It is introduced as an integer jump at a specific epoch (time).

Thus a new relation can be written to describe the observable, that includes the phase ambiguity [3]:

$$\Phi(T)^S = \phi(T) - \phi(T)^S - N^S \quad (2.12)$$

where $\Phi(T)^S$ is the observed phase from the satellite and $\phi(T)$ is the replicated phase and $\phi(T)^S$ is the incoming phase from the satellite. We can rewrite this with the following relation to relate clock time to phase ϕ , nominal phase ϕ_0 , the fundamental frequency f_0 and the time T :

$$f_0 T = \phi - \phi_0 \quad (2.13)$$

Thus with this we can now substitute and rewrite the phase terms with clock times, to later determine the range.

$$\phi(T) = f_0 T + \phi_0 \quad (2.14)$$

$$\phi^S(T^S) = f_0 T^S + \phi_0 \quad (2.15)$$

This forms the following new phase observable [3]:

$$\Phi^S(T) = f_0(T - T^S) + \phi_0 + \phi_0^S - N^S \quad (2.16)$$

By generalizing the observational model we use the following notation:

$$\Phi_k^j(T) = f_0(T_k - T^j) + \phi_{k,0} + \phi_0^j - N_k^j \quad (2.17)$$

Then a conversion from cycles into range has to be done. This is done by multiplying with the carrier wavelength λ_0 and constructing a range measurement $L(T)$ [3].

$$L_k^j = \lambda_0 \Phi_k^j \quad (2.18)$$

$$L_k^j = \rho_k^j + c(dt_k - dt^j) + Z_k^j - I_k^j + \lambda_0 N_k^j \quad (2.19)$$

Notice here the $(-)$ sign in front of the ionospheric term. It means that there is actually a phase advance instead of a delay.

2.4 Single Differencing

The purpose of the single differencing technique is to eliminate the satellite clock bias. Doing this the accuracy if the observation can be improved. Consider two receivers A and B observing one satellite j using the carrier phase observations [3].

$$L_A^j = \rho_A^j + c(dt_A - dt^j) + Z_A^j - I_A^j + \lambda_0 N_A^j \quad (2.20)$$

$$L_B^j = \rho_B^j + c(dt_B - dt^j) + Z_B^j - I_B^j + \lambda_0 N_B^j \quad (2.21)$$

By taking the difference between the two phases we will get the single difference phase ΔL_A^j .

$$\Delta L_{AB}^j = L_A^j - L_B^j \quad (2.22)$$

$$\Delta L(t)_{AB}^j = \Delta \rho(t)_{AB}^j + c \Delta dt(t)_{AB} + \Delta Z(t)_{AB}^j - \Delta I(t)_{AB}^j + \Delta \lambda_0 N(t)_{AB}^j \quad (2.23)$$

It is seen that the satellite clock error term is removed and that all other terms in the observational equation have been differenced and are therefore smaller. For short baselines between receivers both the ionospheric term and the tropospheric term can be considered equal and will cancel out. This can be applied for baseline lengths for less than 30 km (troposphere) and between 1 – 30 km (ionosphere), depending on ionospheric conditions. [3] This makes it possible for us to reduce the equation to:

$$\Delta L(t)_{AB}^j = \Delta \rho(t)_{AB}^j + c \Delta dt(t)_{AB} + \Delta \lambda_0 N(t)_{AB}^j \quad (2.24)$$

From this it can be seen that many error sources have been mitigated or reduced, but to the cost that when taking the difference between the two receivers only their position relative to each other can be estimated.

2.5 Double Differencing

The purpose of double differencing is to eliminate aslo the receiver clock bias. This is done by differencing two single differenced observables, using A and B as index for two receivers and j and k as observed satellites [3]:

$$\Delta L_{AB}^j = \Delta \rho_{AB}^j + c \Delta dt_{AB} + \Delta Z_{AB}^j - \Delta I_{AB}^j + \Delta \lambda_0 N_{AB}^j \quad (2.25)$$

$$\Delta L_{AB}^k = \Delta \rho_{AB}^k + c \Delta dt_{AB} + \Delta Z_{AB}^k - \Delta I_{AB}^k + \Delta \lambda_0 N_{AB}^k \quad (2.26)$$

Then the double differencing is performed by taking the difference of the two single difference observables, which gives the following double difference phase [3]:

$$\nabla \Delta L_{AB}^{jk} = \Delta L_{AB}^j - \Delta L_{AB}^k \quad (2.27)$$

$$\nabla \Delta L(t)_{AB}^{jk} = \nabla \Delta \rho(t)_{AB}^{jk} + \nabla \Delta Z_{AB}^{jk} - \nabla \Delta I_{AB}^{jk} + \nabla \Delta \lambda_0 N(t)_{AB}^{jk} \quad (2.28)$$

Where the super-script (jk) identifies that two satellites has been differenced and ∇ emphasizes that a double difference of two point in the sky has been performed i.e two different satellites [3].

Using double difference has both positive and negative effects: In general compared to single differencing, modeled atmospheric errors are generally increased by a factor of 40 % [3]. Random errors due to multipath and measurement noise is also increased by using this technique. The gain of this technique outweigh these factors, because the size of the clock bias, that we remove, is a much larger errors than these negative increase in the other errors.

2.6 Error Sources

Understanding and correcting for error sources in GPS is important in order to increase the accuracy of the derived results. The following section will describe the different error sources and how they affect the measurements and how they may be eliminated or reduced.

2.6.1 Relativistic effects

Einstein's theory of relativity both general and special will affect the clock of the satellite, due to the satellites velocity in orbit, the change in gravitational potential which is tied to the slight eccentricity in orbit.

To compensate for relativistic effects the satellite's clock frequency is generated slightly lower, this to ensure that the received frequency at the receiver will be the true frequency. The change in eccentricity of the satellite orbit can be compensated for in the receiver by using orbit parameters from the navigational message [1].

$$10.23 \cdot 10^6 \cdot 4.567 \cdot 10^{-9} = 10.22999999545\text{MHz} \quad (2.29)$$

There is also another relativistic effect that affects the accuracy of the position, this is the Sagnac effect, which is induced by the rotation of the earth during the time of the signal transmission. When the receiver solves for the position it solves for a position with a slight offset from the true position due to extra or smaller propagation time. This can induce errors up to 30 m, and is usually compensated for by different techniques. The most common is techniques is that receiver access the time of transmission and subtracts the pseudo range divided by the speed of light from the receivers time marker for the measurement (this after the clock corrections are done). After this the positions from all satellites are calculated and rotation compensated for, by a rotational matrix.

2.6.2 Satellite Clock Errors

All GPS satellites contain four atomic clocks that control everything from signal generation to time stamping the signal. These clocks are highly stable and independent from each other, but they will drift over time due to there inherent structure (nothing is perfect) and age. An offset of just 1ms translates into a accuracy error of about 300 km. The clock errors contains both error in clock drift, relativistic effects, frequency drift clock bias.

The clock error is predicted and overseen by the ground control. They download these clock parameters and tries to predict them, the corrections are then uploaded again to the satellite so they can be transmitted via the navigational message to the receiver that can use them to compensate for the clock errors. This is not prefect, clocks can be modeled with white noise which is inherent extremely hard to predict, so there will always be a residual error in the time measurements from the satellite, this has an affect on accuracy of about 0.3 – 4 m depending on age of the data and type of atomic clocks that are used.

2.6.3 Satellite Orbital Errors

Satellites are positioned accurately in orbit but due to gravitational affects from the sun, moon, solar radiation pressure and orbital maneuvers a slight shift in orbit occurs. This slight change in orbit affects the orbital parameters that determines the orbit and thus its position in relation to the receiver (range). If uncompensated for this will give rise to an error in accuracy. This is compensated for by regularly checking the satellites orbits and sending up corrections to the satellite which transmits them in the navigational message down to the receiver.

This correction is usually computed using a method called kalman filtering, which calculates the satellites future position using its old position, the resulting error is in the range of 2 meter.

2.6.4 Multipath Effects

Multipath affects both the pseudo-range and the carrier phase measurements. This effect comes from the fact that the GPS signal may travels multiple paths to the receiver due to reflections from other structures or natural geometry. When the reflected signals reach the receiver they can cause faults or incorrect correlation peaks in the receiver.

Multipath effects both P and C/A code and produces cycle slips in the data set when the phase lock is lost. The multipath effects on P-code is about a factor of two larger than on C/A - code observations [4]. Multipath influence on carrier phase observations produces a phase shift in the signal and introduces a periodic bias of several centimeters into range observations [4]. This can be modeled roughly as:

$$A_D = A \cos(\Phi_D) \quad (2.30)$$

$$A_R = \alpha A \cos(\Phi_D + \Phi) \quad (2.31)$$

Where A_D and A_R are the amplitudes of the direct and the reflected signals, α is a dampening factor ($0 < \alpha < 1$) and finally Φ_D and Φ is the phase position of the reflected signal and phase shift with respect to the direct signal.

Using superposition we can write these two signals as one signal.

$$A_{signal} = A_D + A_R = A \cos(\Phi_D) + \alpha A \cos(\Phi_D + \Phi) = \beta A \cos(\Phi_D + \Theta) \quad (2.32)$$

This by using $A_{D,max} = A$ and $A_{R,max} = \alpha A$ and where Θ is the multipath error in the in the carrier-phase observations.

$$\Theta = \arctan \left(\frac{\alpha \sin(\Phi)}{1 + \alpha \cos(\Phi)} \right) \quad (2.33)$$

The signal amplitude is described as follows:

$$B = \beta A = A \sqrt{1 + \alpha^2 + 2\alpha \cos(\Phi)} \quad (2.34)$$

By analyzing these equations we can find that the maximum error when using single frequency measurements, L1, is about 5 cm. For linear combinations (L1-L2) this can be larger or smaller due to changing satellite geometry.

Multipath can be reduced by knowing certain aspects of the signal characteristics. For example the reflected signals are much weaker in power when they reach the receiver than the signal that have travelled directly and can thus be filtered away by the receiver. Also

the GPS-signal is right-hand-polarized, the multipath reflections often becomes mainly left-hand-polarized when reflected from surfaces and can also thus be suppressed. An other possibility to reduce the effect is to chose the right geometry of the receiving antenna, such as introducing a ground plane or use a co-centric receiving antenna.

2.6.5 Ionospheric Effects

When a signal propagates through the ionosphere both the modulation of the signal and the carrier is affected, which will introduce a phase advance (negative delay) and a code delay in the signal which affects the measured range from the satellite to the receiver.

The magnitude of the delay is proportional to the electron density in the ionosphere. The electron density changes with the number of dispersed electrons released when gas ionizes due to solar radiation. This density is often integrated in order to obtain the total electron content (TEC).

The ionosphere changes daily and yearly depending on the sun's activity, which ionizes molecules and releases electrons into the atmosphere. This also changes the accuracy of the GPS range measurements which will be further discussed later on in this section.

The satellites elevation angle seen from the receiver is also important for the measurements. If the satellite is at a low elevation angle the signal has to propagate further through the ionosphere and will be more affected by it.

The ionosphere has a property that helps us combat it. It is frequency dependent (dispersive). This means that it will affect different frequencies by introducing different delays, which also means that the code and carrier phase measurement will be affected differently at the two carriers L1 and L2. The carriers phase will be advanced and the code modulation will be delayed.

To sum up the ionosphere affects higher frequencies less than lower frequencies. This gives us the tools to eliminate or reduce it, by using linear combinations of the two frequencies, which will reduce the influence by the ionosphere by 99.9 % [1]. This is done in the following way [1]:

$$I_k^j = \frac{40.3}{cf^2} TEC \quad (2.35)$$

where ΔL is the delay of the ionosphere due to its total electron count and frequency.

$$L_1 = L_3 + \Delta L_1 ; L_2 = L_3 + \Delta L_2 \quad (2.36)$$

$$f_{L1}^2 \times L_1 - f_{L2}^2 \times L_2 = (f_{L1}^2 - f_{L2}^2) \times L_3 \quad (2.37)$$

Using linear combinations we can rewrite the equation and solve for L_3 , which has almost no ionospheric influence [1].

$$L_3 = \frac{f_{L1}^2}{(f_{L1}^2 - f_{L2}^2)} L_1 - \frac{f_{L2}^2}{(f_{L1}^2 - f_{L2}^2)} L_2 = 2.5L_1 - 1.5L_2 \quad (2.38)$$

2.6.6 Tropospheric Effect

The troposphere is the lower part of the atmosphere. The troposphere is a non-dispersive media which means that it has no frequency dependence. This means that the troposphere will affect both the code and the carrier phase measurement in the same way by delaying them the same amount.

The delay in the troposphere is a function of the refractive index which depended on local conditions such as temperature, pressure and relative humidity. If not compensated

for this will induce an error of about 2.4 m in the zenith direction. Thus it can be expressed by integrating over the signal path through the troposphere. [1]

$$Z = \int (n - 1) ds = 10^{-6} \int N^{trop} ds \quad (2.39)$$

where n is the refractive index and $N^{trop} = 10^{-6}(n - 1)$ is the refractivity.

The refractive index is often modeled as dry and wet components (hydrostatic, non-hydrostatic) or ZHD and ZWD. The ZHD component stands for about 90 % of the total delay in the troposphere. ZWD arises from the water vapor in the atmosphere, this is usually more complicated to model due to the fact that the amount of water vapor in the atmosphere varies locally. But this can be expressed using the Hopfield model (1969), where the dry and wet contribution are separated accordingly [7].

$$N^{trop} = N_{zhd}^{trop} + N_{zwd}^{trop} \quad (2.40)$$

This can then be expanded into the following model, introducing both a vertical height dependance and a elevation dependent mapping functions. [7]

$$Z = \frac{10^{-6}}{5} [N_{zhd,0}^{trop} h_{zhd} m_{zhd}(\varepsilon) + N_{zwd,0}^{trop} h_{zwd} m_{zwd}(\varepsilon)] \quad (2.41)$$

where h is the height in meters and $m(\varepsilon)$ is the elevation dependent mapping function. The mapping functions have a geometric interpretation, depending on the zenith angel of the signal, as follows [7].

$$m_{zhd}(\varepsilon) = \frac{1}{\sin \sqrt{\varepsilon^2 + 6.25}} \quad (2.42)$$

$$m_{zwd}(\varepsilon) = \frac{1}{\sin \sqrt{\varepsilon^2 + 2.25}} \quad (2.43)$$

where ε is the elevation angle of the line of sight path.

2.6.7 Satellite Geometry

The satellite geometry is often referred to as the dilution of precision which is a value describing the satellite geometry. Because the satellite geometry is a very important factor for the accuracy for the position derived from the pseudo-range observations. This comes from that the geometry changes with time due to the relative motion of the satellites in orbit. The satellite geometry can be described using what are called DOP-factors which are simple linear function obtain from the diagonal elements of the co-factor matrix of the adjusted position parameters from the position solution.

So the accuracy of the GPS measurements can be summarized into these two points:

- Accuracy of single pseudo-range measurement, expressed by the standard deviation.
- The geometric distribution of the satellites in use.

The observed pseudo-range accuracy is related to the accuracy of the final observations by the scalar DOP factor. Where a good geometry should be mirrored by a low DOP value.

$$\sigma = DOP \cdot \sigma_{obs} \quad (2.44)$$

The different DOP factors can be computed using the co-factor matrix, which is built from the design matrix of the position adjustment solution, accordingly:

$$Q_X = (A^T A)^{-1} = \begin{pmatrix} \sigma_{xx}^2 & \sigma_{xy} & \sigma_{xz} & \sigma_{xt} \\ \sigma_{yx} & \sigma_{yy}^2 & \sigma_{yz} & \sigma_{yt} \\ \sigma_{zx} & \sigma_{zy} & \sigma_{zz}^2 & \sigma_{zt} \\ \sigma_{tx} & \sigma_{ty} & \sigma_{tz} & \sigma_{tt}^2 \end{pmatrix}$$

where $X = \{x_k, y_k, z_k, t_k\}$. There are different types of DOP-factors which describes accuracy in different dimensions. They are taken accordingly from the diagonal elements of the co-factor matrix:

Table 2.4: Different DOP-factors for different dimensions.

$\text{GDOP} = \sqrt{\sigma_{xx}^2 + \sigma_{yy}^2 + \sigma_{zz}^2 + \sigma_{tt}^2}$	Geometric dilution of precision
$\text{PDOP} = \sqrt{\sigma_{xx}^2 + \sigma_{yy}^2 + \sigma_{zz}^2}$	Position dilution of precision
$\text{TDOP} = \sqrt{\sigma_{tt}^2}$	Time dilution of precision

2.6.8 Receiver Noise and Clock Error

There is an error in the receiver clock that generates the replica signal. This error varies with the receiver quality and with the frequency standard, but can be compensated for using the differencing technique. The receiver also have internal noise the comes from the electronics. They are quite small, in the range of, for code measurement about 1 % of the wavelength and for carrier phase measurement an error of about 1 mm.

2.7 Geophysical Model and Reference System

In the satellite positioning systems we have two kinds of coordinates systems, the first one being an inertial system, the second a rotational system. To understand the navigation problem we have to define coordinate systems so we can uniquely define positions in spacial coordinates where both the state of satellite and the receiver can be represented.

For the satellite an inertial frame of reference is the best. This frame is called the Earth Centered Inertial coordinate system or ECI. The system describes the motion of the satellit in relation to the Earth, where the horizontal-plane coincides with the equatorial plane and the x-axis in a specific direction in the celestial sphere. The z-axis is taken to be the normal to the horizontal-plane (the xy -plane) thus in the direction of the north pole, the y-axis is taken in order to form a right handed coordinate system. This system is not totally inertial, due to the sun's and the moon's gravitational pull and because of the earth rotation our planet is not a prefect sphere, it is an ellipsoid. So the system wobbles in relation to the x and z-axis definitions of direction. This can be corrected by introducing a direction in time, which means that in our case the x-axis is defined to point at the vernal equinox at a precise instant in time or epoch, which is 12:00 hours UTC or the 1:st of January 2000.

For the receiver it is more convenient to use a coordinate system that rotates with the earth, this makes it easier to calculate the latitude, longitude, and height parameters. This is called the Earth Centered Earth Fixed coordinate system, or ECEF. In this system the (x, y, z) axis rotates with the earth and are no longer fixed in an inertial frame. The axes are defined almost as before, horizontal-plane in the equatorial plane, +x-axis at the 0 degree longitude, +y-axis at the 90 longitude, and the z-axis as the normal to the horizontal-plane, thus in the direction of the geographical north pole. The geophysical model used for GPS is called the World Geodetic System 1984 (WGS 84). This model contains detailed information about the Earth's gravitational irregularities. It is based on the fact the the Earth is an ellipsoid and modeled after that. However there are many models that describe the gravitational field of the Earth, WGS 84 is just one of them. The newest model is the International Terrestrial Reference Frame (ITRF). This model includes atmospheric and oceanic loading and it models all the earth mass, not just the bedrock. It also has the feature of no-net-rotation. Which means that all the tectonic plates are moving but when compared to the whole picture they have a no net rotation.

To transform between the inertial and the rotational frame a rotation matrix is applied, that compensates for the different factors between the two coordinated systems.

$$x_i = P \cdot N \cdot S \cdot W \cdot x_t \quad (2.45)$$

The parameter P is the Precession, N the nutation, S the spin, and W the polar motion.

In general it is always necessary to transform the position that is solved from the GPS observations into a local or national reference system. There are not just international reference systems. There are also national ones differing from each other by centimeters to decimeters. For the usual GPS applications this do not introduce a problem. The different system are connected to each other, many looking very much alike. The WGS 84 reference frame is for example connected to the ITRF system.

2.8 Point Positioning using Pseudo-range

To solve the point position problem we start by linearising the pseudo-range observable. We use the least square approach to solve for the point position. We start to define the actual observations as a model with added noise as follows [3]:

$$P_{observed} = P_{model} + v \quad (2.46)$$

Once this is done we linearise the model using a Taylor expansion, ignoring all higher order terms [3].

$$P(x, y, z, \tau) = P(x_0, t_0, z_0, \tau_0) + \Delta x \frac{\delta P}{\delta x} + \Delta y \frac{\delta P}{\delta y} + \Delta z \frac{\delta P}{\delta z} + \Delta \tau \frac{\delta P}{\delta \tau} \quad (2.47)$$

where $\Delta(x_0, y_0, z_0, \tau_0)$ are provisional parameters. [3]

$$\Delta x = x - x_0 \quad (2.48)$$

$$\Delta y = y - y_0 \quad (2.49)$$

$$\Delta z = z - z_0 \quad (2.50)$$

$$\Delta \tau = \tau - \tau_0 \quad (2.51)$$

From this we can define the residual observations ΔP to be the difference between the measured observables and the computed observables from the model [3].

$$\Delta P = P_{observable} - P_{computes} \quad (2.52)$$

or

$$\Delta P = \Delta x \frac{\delta P}{\delta x} + \Delta y \frac{\delta P}{\delta y} + \Delta z \frac{\delta P}{\delta z} + \Delta \tau \frac{\delta P}{\delta \tau} + v \quad (2.53)$$

This linearised system can then be generalized for multiple observations using matrix notation, as follows [3]:

$$\mathbf{b} = \mathbf{A}\mathbf{x} + \mathbf{v} \quad (2.54)$$

where \mathbf{b} is the residual observations, \mathbf{A} is the linear design matrix, containing the partial derivatives with respect to each parameter, \mathbf{x} is the unknown correction parameters that we want to solve for, and v is the noise terms.

To solve this linear system we introduce the least square concept. The estimated residuals are defined as the difference between the observed residuals and computed residuals from the model. Then we can write the linearised observation equations for the estimated residuals as:

$$\hat{\mathbf{v}} = \hat{\mathbf{b}} - \mathbf{A}\hat{\mathbf{x}} \quad (2.55)$$

The least square solution can be computed by varying the value of $\hat{\mathbf{x}}$ until the function of the squared residuals is minimized [3]:

$$J(\hat{\mathbf{x}}) = \sum_{i=1}^m v^2 = (\mathbf{b} - \mathbf{A}\mathbf{x})^T (\mathbf{b} - \mathbf{A}\mathbf{x}) \quad (2.56)$$

The solution is obtained when when $J(\hat{\mathbf{x}})$ becomes stationary when varying $\hat{\mathbf{x}}$, since the derivative of the function should be zero. Rewriting this function we can obtain the system of the so called "normal equations" and the solution of the normal equations is as follows [3]:

$$\hat{\mathbf{x}} = (\mathbf{A}^T \mathbf{A})^{-1} \mathbf{A}^T \mathbf{b} \quad (2.57)$$

2.9 Relative Positioning using carrier phase

The objective of relative positioning is to determine the coordinates of a unknown point with respect to a known point. This is done by forming what is called a baseline vector between the two points.

$$\vec{X}_A = \vec{X}_B + \vec{B}_{AB} \quad (2.58)$$

Thus the baseline vector becomes:

$$\vec{B}_{AB} = \begin{pmatrix} X_B - X_A \\ Y_B - Y_A \\ Z_B - Z_A \end{pmatrix} = \begin{pmatrix} \Delta X_{AB} \\ \Delta Y_{AB} \\ \Delta Z_{AB} \end{pmatrix}$$

2.9.1 Kinematic relative position

In this type of relative positioning we keep one of the stations fixed while the other one moves and its position has to be determined at different epochs. This concept is built around the notion that the geometric distance is changing with the motion of the stations/receivers and can be described by the same true range description formulated in the pseudo-range and carrier phase sections [1].

$$\rho_B^j = \sqrt{(X^j(t) - X_B(t))^2 + (Y^j(t) - Y_B(t))^2 + (Z^j(t) - Z_B(t))^2} \quad (2.59)$$

The kinematic case can be described by the the following true range description where a time dependence due to motion has been introduced in the coordinates. Where the j is the satellite and $k = B$ is the station point.

2.10 Linear dependence of observations

We have in previous sections described single and double difference (SD and DD) techniques of observations to reduce the impact of inherent error sources in the observations. However, these techniques give rise to some considerations themselves. One of these are linear dependence of observations which comes from that there are more possible ways to combine the observations than there are actual observations.

We can form many of these double difference combinations by just differencing other double difference pairs. This can be demonstrated by using three satellites and two receivers (j, k, l and A, B) which forms the following DD-pairs [3]:

$$L_{AB}^{jk} = (L_A^j - L_B^j)(L_B^k - L_B^k) \quad (2.60)$$

$$L_{AB}^{jl} = (L_A^j - L_B^j)(L_B^l - L_B^l) \quad (2.61)$$

$$L_{AB}^{lk} = (L_A^l - L_B^l)(L_B^k - L_B^k) \quad (2.62)$$

Form these three DD-pairs we can form the following DD-observations by linear combination [3]:

$$L_{AB}^{jk} = L_{AB}^{jl} - L_{AB}^{lk} \quad (2.63)$$

$$L_{AB}^{jl} = L_{AB}^{jk} - L_{AB}^{lk} \quad (2.64)$$

$$L_{AB}^{lk} = L_{AB}^{jk} - L_{AB}^{jl} \quad (2.65)$$

This can be generalized into one equation, when double difference observations (pairs) are used:

$$N_{LC} = \frac{1}{2} \cdot N_{DD} \cdot (N_{DD} - 1) \quad (2.66)$$

where N_{LC} is the number of linear combinations created from the total number of double difference pairs N_{DD} . To solve the "normal equations" using the least square approach we need to have linearly independent set of SD or DD-pairs otherwise the least square approach will not give a unique solution.

3 Time Series Analysis

In this chapter we will introduce the theory that will help us analyze an treat time series both in the time and frequency domain. We will focus on statistical and spectral analysis and introduce ways to characterize the results

3.1 Statistical Analysis

In this section we will present statistical tools to be used in the thesis to estimate characteristics of time series and the information they contain.

3.1.1 Arithmetic Mean

The arithmetic mean of a set of numbers tell us what the central tendency of a set of numbers (sample space) are. If we have a sample space of $\{x_1, \dots, x_N\}$ then the following arithmetic mean is computes as follows [6]:

$$\mu_x = \frac{1}{N} \sum_{i=1}^N x_i \quad (3.1)$$

where N is the number of samples. The arithmetic mean or sample mean is usually a very good choice to explore a central tendency in a set of samples. However, it may be influenced by outliers, that may be removed before the μ_x is computed, to give a accurate description of the central tendency.

A second measure of central location of a random variable is the median. If the random variable is continuous the median is the halfway point. Let $\{x_1, x_2 \dots x_n\}$ be samples of observations arranged in the order from the smallest to the largest. Then the sample median is the middle observation of n , if n is odd, if n is even the sample median is the mean value of the two middle observations.

In this thesis we will use the symbol $\tilde{\mu}_x$ and the center location will be described by the following relation:

$$\text{center location} = \frac{n+1}{2} \quad (3.2)$$

3.1.2 Variance and Standard Deviation

The variance is a measure of how far numbers or points a spread out from a mean value [6].

$$\sigma^2 = \frac{1}{N-1} \sum_{i=1}^N (x_i - \mu_x)^2 \quad (3.3)$$

Variance has no unit and is thus unit less. We introduce also the standard deviation which is defined as the square-root of the variance [9]:

$$\sigma = \sqrt{\text{Var}(x)} = \sqrt{\sigma^2} \quad (3.4)$$

The standard deviation is here a measure of variability. It is a positive number and has the advantage that it has the same unit as the original data. A high standard deviation indicates a high unstability or spread of data points, and makes it hard to predict (high variability). An low standard deviation is an indication of stability and small spread of data points [9].

Minimizing the variance is often the main focus of many processing techniques to reduce noise in data. Because if the variance is minimized the spread of data about the mean value is lower, thus a better description is made of the data.

3.1.3 Root Mean Square (RMS)

Root mean square is also known as the quadratic mean and is a measure of magnitude of a changing variable. The RMS can be expressed as the variation around a average value as follows:

$$RMS = \sqrt{\mu^2 + \sigma^2} \quad (3.5)$$

where μ is the arithmetic average and σ is the standard deviation. From this relation it is clear that the RMS is always equal to or larger than the mean. For many physical applications the mean is usually removed just because sometimes it is more valuable to see the change around a fitted model or line. This reduces the RMS to be equal to the standard deviation.

$$RMS = \sigma \quad (3.6)$$

3.1.4 Correlation

Correlation, or in this case the correlation coefficient, is a measure of the linear dependence of two variables x and y . The correlation coefficient tells us how strong the linear dependence is between the variables. One way to determine the correlation coefficient is to use the "Pearson coefficient of correlation" [9]. It is defined as follows: Let x and y be random variables with mean μ_x and μ_y and standard deviations σ_x and σ_y . The correlation ρ_{xy} between x and the y is then given by [9]:

$$\rho_{xy} = \frac{\text{Cov}(x, y)}{\sigma_x \sigma_y} \quad (3.7)$$

where $\text{Cov}(x, y)$ is the covariance and E is the expectation of the product of the two parameters minus the mean.

$$\text{Cov}(x, y) = E[(x - \mu_x)(y - \mu_y)] \quad (3.8)$$

The correlation coefficient ranges from -1 to 1 . Where the value 1 indicates that a linear function fits the relationship between X and Y perfectly. A positive correlation coefficient indicates that data points on or around a linear function gives a increase in both X and Y . While a negative correlation coefficient implies that data points around or on the negative linear function gives a decrease in Y when X increases. A correlation coefficient of 0 indicates no linear correlation between the two parameters. Note that 0 correlation does not mean that the variables are unrelated. It only means that there is no linear dependence between two variables [9].

3.1.5 Linear Regression and Residuals

Linear regression attempts to model the relationship between two variables, one scalar variable and one dependent variable, by fitting a linear function to observed data. In a simple linear regression data is fitted using a least square estimator where the residuals of the linear function that is fitted so that the sum of the square residuals are minimized. This approach is used when there is non-stationarity in data with a linear dependence to either estimate the trend in the data set or to remove it, by removing the the linear model from the observed data points (usually called de-trending).

First we assume that we have a set of data points $\{y_i, x_i\}$ ($i=1,2,\dots,n$) to which we want to fit the following linear function:

$$y = \beta_0 + \beta_1 x \quad (3.9)$$

where β_0 is the intercept point and β_1 is the slope of the linear function.

To provide the best fit for this function to the observed data set we use a least square estimate to find the best estimate of the intercept point and slope. This is done by minimizing the sum of the squared residuals, usually called SSE (sum of square errors), in this paper we are going to use the same notation as in 2.48, where $\text{SSE}(\beta_0, \beta_1) = J(\beta_0, \beta_1)$.

$$J(\beta_0, \beta_1) = \sum_{i=1}^n e_i^2 = \sum_{i=1}^n (y_i - \beta_0 - \beta_1 x)^2 \quad (3.10)$$

By differentiating $J(\beta_0, \beta_1)$ with respect to both parameters β_0, β_1 and then setting the partial derivatives to zero we get the following:

$$\frac{\partial J}{\partial \beta_0} = \sum_{i=1}^n y_i \quad (3.11)$$

$$\frac{\partial J}{\partial \beta_1} = \sum_{i=1}^n x_i y_i \quad (3.12)$$

These are called the normal equations and where the estimates of β_0 and β_1 becomes:

$$\beta_1 = \frac{n \sum_{i=1}^n x_i y_i - (\sum_{i=1}^n x_i) (\sum_{i=1}^n y_i)}{n \sum_{i=1}^n x_i^2 - (\sum_{i=1}^n x_i)^2} \quad (3.13)$$

$$\beta_0 = \bar{y} - \beta_1 \bar{x} \quad (3.14)$$

where the bars over the variables is the sample mean (arithmetic mean). Now we can set up a relation for the residual or de-trended time series as follows:

$$e_i = y_i - (\beta_0 + \beta_1 \bar{x}) \quad (3.15)$$

$$e_i = y_i - \bar{y} \quad (3.16)$$

To summarize we will talk about the properties of the least square estimators and the model assumptions.

Table 3.1: Model assumptions for simple linear regression

– y_i is a linear independent random variable with a normal distribution.
– The mean of y_i is $(\beta_0 + \beta_1 x)$.
– The variance of y_i is σ^2 .

Then model assumptions for a simple linear regression can be described from 3.1 in this form.

$$y_i \sim N(\beta_0 + \beta_1 x, \sigma^2) \quad (3.17)$$

Thus the residuals properties can be described from 3.2 in the following form

$$e_i \sim N(0, \sigma^2) \quad (3.18)$$

Table 3.2: Properties of residuals least square estimates

– Sum of squared residuals are zero
– The mean of the residuals are zero
– e_i are assumed to have normal distribution
– Variance of e_i is σ^2

3.1.6 Histogram

A histogram is a statistical representation of the inherent distribution of a data set and is usually used to estimate the probability density function of the underlying variable. In a histogram we can illustrate the following properties of a distribution:

- center location of data
- standard deviation (spread)
- outliers
- multiple modes

By defining a function m_i that counts the number of observations that fall into a specific range, called bins, we can form the following mathematical representation of a histogram.

$$n = \sum_{i=1}^k m_i \quad (3.19)$$

where n is the number of observations and k is total number of bins.

To estimate the bin width k there are number of different approaches, we will only use one them here. The bin width of a histogram can by rule of thumb be estimated using approximately by:

$$k = \left\lceil \frac{\max(x) - \min(x)}{h} \right\rceil \quad (3.20)$$

where $\lceil \]$ indicates the ceiling function, h is the suggested bin width, $\max(x) - \min(x)$ gives the range of the data. Calculating the bin width we use the following approximation:

$$h = \frac{3.5\sigma}{n^{1/3}} \quad (3.21)$$

where n is the number of samples or data points and σ is the standard deviation.

3.2 Spectral Analysis

In this section we will present tools to estimate spectral properties of the time series and to characterize the signals contained in the time series.

3.2.1 Power Spectral Density

The main reason for spectral estimation is to find and study the distribution of power contained in a signal or sample data set over specific frequencies. Where the signal has a finite length. This is generally done by estimating the "Discrete Fourier transform" or DFT of the signal, the DFT is usually computed using a "Fast Fourier transform" (FFT).

This spectral estimate is usually called the periodogram or the power spectral density (PSD).

First we estimate the DFT of the finite length signal:

$$X(w) = \sum_{n=-\infty}^{\infty} x[n]e^{j\omega n} \quad (3.22)$$

This can be expressed in a physical frequency by using the relation:

$$\omega = \frac{2\pi f}{f_s} \quad (3.23)$$

where f_s is the sampling frequency.

$$X(f) = \sum_{n=-\infty}^{\infty} x[n]e^{j2\pi n f / f_s} \quad (3.24)$$

To estimate the PSD the magnitude of the DFT is computed and then squared. Computing the magnitude squared (power) makes the PSD a positive entity this is called the one-sided PSD. The estimated power is then scaled with the length N and the sampling frequency f_s and multiplied by a factor of 2. This to correct for the power contained in the negative frequencies [8].

$$P_{xx}(f) = \frac{2}{f_s N} |X(f)|^2 \quad (3.25)$$

One of the properties of the power spectral density is that the variance can be estimated from integration over the whole range of the PSD.

$$\sigma^2 = \int_0^f P_{xx}(f) df \quad (3.26)$$

This is stated from Parseval's theorem which says that the power estimated in the time domain must be equal the power in the frequency domain, thus also the variance.

The frequency resolution of the power spectral density estimate is proportional to the number of samples N . The frequency resolution δ_f for the discrete case is calculated as follows.

$$\delta_f = \frac{f_s}{N} \quad (3.27)$$

where f_s is the sampling frequency and N is the number of samples.

3.2.2 Integrated Power

The total power in the time-series using a one-sided the power spectral density is estimated by using Parseval's Theorem. It states that the total power contained in a PSD is the integrated area under the PSD function.

$$P_{tot} = \int_0^f P_{xx}(f) df \quad (3.28)$$

The power contained in different frequency bands can be estimated by integrating over the specific frequencies in power spectral density estimate.

$$\vec{P}_{ij}(f_{ij}) = \int_{f_i}^{f_j} P_{xx}(f)df \quad (3.29)$$

where i, j are frequency indices ranging from $\{0, 1, \dots, N\}$, where N is the number of samples. The frequency resolution of the integrated power in the different frequency bands (frequency bins) is $\delta_f = f_j - f_i$, which is equal the bin width f_{ij} . It is important to note that the frequency bins have to be of the same size, in order to estimate the correct integrated power.

3.2.3 Trapezoidal Numerical Integration

One of the methods of integration that can be used is the trapezoid numerical integration method, which is defined as follows.

$$F(x) = \int_b^a f(x)dx = (b - a) \cdot \left[\frac{f(a) + f(b)}{2} \right] \quad (3.30)$$

Substituting the trapezoidal numerical integration method instead for the integral we get the following relation for P :

$$P_{avg} = (f_2 - f_1) \cdot \left[\frac{P_{xx}(f_1) + P_{xx}(f_2)}{2} \right] \quad (3.31)$$

The trapezoidal rule for numerical integration is a technique for approximating a definite integral. It works by approximating the the area under the graph of the function as trapezoid. The trapezoidal integration method is especially accurate and converge fast for periodic functions, when integrated over there whole period. This due to the inherent symmetry of periodic functions which makes errors to cancel out.

3.2.4 Noise and Signal Power Estimation

We want to define some way to identify and estimate noise power in our time series, this accomplished by choosing what signal components, that we want to keep. By analyzing the PSD estimate we can get a sense of where our signals are located in the frequency spectrum. By choosing a frequency band that we define as our signal bandwidth, everything outside this band can be considered noise. We also want to define the same way to determine signal power in our time-series, this is done in same way as for noise power, by defining a signal band (SB).

This is done by defining the signal frequency bandwidth as f_{SB} and then defining the frequency noise band. The noise frequency band, for our application, can be defined by two sub-bands f_{SN1} and f_{SN2} .

$$\begin{cases} f_{SB} = \{f_1, f_2\} \\ f_{SN1} = \{f_0, f_1\} \\ f_{SN2} = \{f_2, f_n\} \end{cases} \quad (3.32)$$

$$P_{noise} = \int_{f_0}^{f_1} P_{xx}(f)df + \int_{f_2}^{f_n} P_{xx}(f)df \quad (3.33)$$

$$P_{signal} = \int_{f_1}^{f_2} P_{xx}(f)df \quad (3.34)$$

We can also define a measure of reduction in noise by applying the noise estimation procedure on for example filtered and unfiltered data by the following relation:

$$\chi_{noise} = 100 \cdot \left(1 - \frac{P_{noise,1}}{P_{noise,2}} \right) \quad (3.35)$$

where $P_{noise,1}$ is a filtered time series and $P_{noise,2}$ is the original time series. The answer will then be presented in percent (0–100 %) where 0 % indicates no reduction in noise.

The same can be done for the signal band as follows with the same properties as for the noise band.

$$\chi_{signal} = 100 \cdot \left(1 - \frac{P_{signal,1}}{P_{signal,2}} \right) \quad (3.36)$$

A way to measure the influence of wanted and unwanted signals is the "Signal-to-Noise Ratio" or the "SNR", which is defined as the ratio between the power of the signal and the background noise in the time-series.

$$SNR = \frac{P_{signal}}{P_{noise}} \quad (3.37)$$

where a ratio higher than one indicates more signal than noise. Which means more concrete that the signal can be stronger than the noise and can be easily distinguished from the noise. Due to the fact that the dynamical range of frequencies can be large the SNR is usually described in a logarithmic scale, in the form of decibels.

$$SNR = 10 \log_{10} \left(\frac{P_{signal}}{P_{noise}} \right) \quad (3.38)$$

4 Time Domain Filtering

In this section we will introduce the ordinary sidereal filtering approach and how it works and then move on to the reduced sidereal filter which was developed for this thesis. Further we will present a model that will be used to theoretically determine the change of standard deviation or the RMS in the geodetic time-series. When the two filtering approaches are applied.

4.1 Sidereal Filtering

The sidereal filtering technique uses the fact that the geometry between the GPS satellite and the receiver on the ground repeats itself roughly every sidereal day (23 h 56 m 04 s). The repeating geometry means that common mode signals are introduced into the time series which has a corresponding sidereal repeating period as the geometry of the GPS satellites. This repeatability can be used to mitigate the common mode signals or induced errors (such as signal multipath).

This roughly means that one epoch is approximately the same as the epoch shifted by one sidereal period/day away. Described as follows:

$$X(t) \cong X(t + \tau) \quad (4.1)$$

where $\tau = 23 \text{ h } 56 \text{ m } 04 \text{ s}$, which will be called the sidereal time shift, and $X(t)$ is the position estimate at a specific epoch. From this we can construct a sidereal filter by using a minimum of two days to form the following time domain filters:

$$F_{1,2} = \frac{1}{2} \cdot [X_1(t) + X_2(t + \tau)] \quad (4.2)$$

This can be generalized to the following equation:

$$F_{k,k+n} = \frac{1}{2} \cdot [X_k(t) + X_{k+n}(t + \tau)] \quad (4.3)$$

Then applying this to the days of the time series we get the filtered observations:

$$X_k^F(t) = X_k(t) - F_{k,k+n}(t) \quad (4.4)$$

where $X_k^F(t)$ are the filtered observations of $X_k(t)$.

4.2 Reduced Sidereal Filtering

In the original sidereal filtering approach noise and signals are mapped (it is a smoothed copy of the unfiltered day) into the filter when it is constructed. This approach has when applied onto the original time series a mitigating affect on both high and low frequency components. This means that it reduces both the power of the signals in the time series as well as the noise (which we want to remove). This can be showed by setting up the following signal structure:

$$y(t) = x(t) + v(t) \quad (4.5)$$

$$y_{sdf}(t) = a[x(t) + v(t)] \quad (4.6)$$

where $\Delta y(t) = y(t) - y_{sdf}(t)$, $v(t)$ is the noise term and $x(t)$ is the signal of interest.

$$\Delta y(t) = (1 - a)[x(t) + v(t)] \quad (4.7)$$

Regular sidereal filtering affects, as can be seen in 4.7, both the signal and the noise with the same amount. In most applications we want to preserve the signal and reduce noise. This obstacle can be overcome by removing, in the sidereal filter, the frequency components containing the signal. This by applying a digital filter to the sidereal filter. Doing so will preserve the signal in the time series when the time domain filtering (differencing of $X(t) - F(f)$) is applied. This can be mathematical shown as follows, by noting the following signal structure:

$$y(t)_{sdf} = x(t) + v(t) \quad (4.8)$$

By setting $y(t)_{sdf}|_{x(t)=0}$ (removing the signal components) we get the following relation.

$$y_{sdf}(t) = a \cdot v(t) \quad (4.9)$$

$$\Delta y(t) = x(t) + (1 - a)v(t) \quad (4.10)$$

From this it can be seen that the original signal $x(t)$ is kept unaffected and the noise is reduced by a factor of $(1 - a)$. By transforming the sidereal filter into the frequency domain we can write an expression for the reduced sidereal filter:

$$F(t) \rightarrow \{\mathcal{F}(F(t))\} \rightarrow F(j\omega) \quad (4.11)$$

where ω stands for the angular frequency, $H(j\omega)$ is the filter implementation to the sidereal filter and \mathcal{F} is the Fourier transform. Now we can write the equation for the reduced sidereal filter as follows in the frequency domain:

$$F_k^F(j\omega) = H(j\omega)F_{k,k+n}(j\omega) \quad (4.12)$$

5 Frequency Domain Filtering

In this chapter we will present basic digital filter theory of the notch filter and how it's designed and realized.

5.1 IIR Filter Design

Frequency domain filtering can be described by using the concept of linear systems where a input signal is affected by a frequency selective filter. The output signal is then reshaped by the digital filter according to specifications. The system response can be described in the frequency domain.

$$Y(z) = H(z)X(z) \quad (5.1)$$

where $Y(z)$ is the output signal, $X(z)$ is the input signal and $H(z)$ is the filter.

The filter $H(z)$ is usually described by the generic transfer function [2].

$$H(z) = \frac{Y(z)}{X(z)} = \left(\frac{b_0 + b_1z^{-1} + \dots + b_mz^{-m}}{1 + a_1z^{-1} + \dots + a_nz^{-n}} \right) \quad (5.2)$$

Frequency domain terminology gives a simple description of the frequency selective bands and filter characteristics. There are three main bands in general, called the stop-band, passband and transitionband. The stopband is the frequency range where frequencies are attenuated. The passband the range of frequencies where the signal is passed without any, or with small, attenuation. Further characteristics of the filter is the filter order. Which controls the rolloff characteristics, describing the change between the stop and pass band. This controls the size of the transition band. The transition band describes the range of frequencies that are unwittingly affected by the filter. Now we want to find the relations of magnitude response $M(w)$, phase response $\phi(w)$, and group delay $\tau_g(w)$. They can be calculated as follows [2]:

$$M(w) = -20 \cdot \log(|H(j\omega)|) \quad (5.3)$$

$$\phi(w) = -\arg[|H(j\omega)|] \quad (5.4)$$

$$\tau_g(w) = \frac{\partial\phi(\omega)}{\partial\omega} \quad (5.5)$$

$M(w)$ is the magnitude response of the filter which measures the size/magnitude of the signal as function of frequency. $\phi(w)$ is the phase response of the filter and measure of the phase of the signal changes over frequency, and τ_g is the rate of change of phase over angular frequency. Thus this can be used as a measure of signal distortion introduced by the filter. This comes from the fact that the propagation velocity changes with frequency. Therefore group velocity tends to peak near the cutoff frequency resulting in phase distortion.

5.1.1 Notch Filter Design by Pole-Zero Placement

The notch filter is a frequency selective filter specialized in removing a of a single or narrow band of frequencies. It can be seen as a special case of the bandstop filter where the stopband goes to zero. Notch filtering has the desire to remove a specific center frequency called f_0 also called the notch frequency [10]. The frequency response an ideal notch filter can be described as follows.

$$H_{notch}(f) = 1 - \delta_0(f - f_0) \quad (5.6)$$

where δ_0 is the unit impulse response and $(0 < f < f_s/2)$.

The design of the notch filter is done by placing a zero on the unit circle on the point corresponding to the notch frequency f_0 . The angle associated with this point can be computed and makes f varies between 0 and $f_s/2$.

$$\Phi_o = \frac{2\pi f_0}{f_s} \quad (5.7)$$

where f_s is the sampling frequency.

By placing a zero at $z = e^{j2\pi f_0}$ will ensure that $H_{notch}(f_0) = 0$. To control the bandwidth of the notch filters stop-band we place a pole at Φ_0 inside the unit circle, thus $r < 1$, where r is, if $\Delta f \ll f_0$ (Δf is the filter bandwidth), the pole radius is:

$$r \approx 1 - \frac{\Delta f \pi}{f_s} \quad (5.8)$$

Using this and that poles and zeros must be in complex-conjugate pairs, will give the following transfer function for the notch filter.

$$H_{notch}(z) = \frac{b_0[z - e^{j\Phi_0}][z - e^{-j\Phi_0}]}{[z - re^{j\Phi_0}][z - re^{-j\Phi_0}]} \quad (5.9)$$

and by using Euler's identity we can reduce the transfer function down to

$$H_{notch}(z) = \frac{b_0(z^2 - 2\cos(\Phi_0)z + 1)}{(z^2 - 2r\cos(\Phi_0)z + r^2)} \quad (5.10)$$

where the two control parameters to be determine are the gain b_0 and the pole radius r .

5.1.2 Analog to Digital Conversion

To convert a analog filter into a digital filter (from a continuous-time filter to a discrete-time filter) a bilinear transformation is done. This transformation preserves the stability of the analog filter and maps every point in frequency response in the analog filter into a corresponding point in the frequency response of the digital filter (1:1 mapping). This with only a very small frequency shift [11].

$$\omega' = \frac{2}{T} \cdot \tan\left(\frac{\omega T}{2}\right) \quad (5.11)$$

Applying this bilinear transformation by replacing ω with ω' we get the following digital filter:

$$H(j\omega')_D = H\left(j\frac{2}{T} \cdot \tan\left(\frac{\omega T}{2}\right)\right)_A \quad (5.12)$$

5.2 IIR Filter Realization

The IIR filter is characterized by a rational fractional transfer function based on zeros and poles, using the z-transform. With the generic transfer function of n :th order [10]:

$$H(z) = \frac{(b_0 + b_1z^{-1} + \dots + b_mz^{-m})}{(1 + a_1z^{-1} + \dots + a_nz^{-n})} \quad (5.13)$$

where $m = n$ to give the transfer function the same polynomial degree both in the denominator and numerator. There are a number of ways to realize this transfer function and one of these methods will be presented in the following sections.

5.2.1 Direct Form I

The simplest realization of $H(z)$ is based on factoring the transfer function into autoregressive moving average parts [10] as follows:

$$H(z) = \left(\frac{1}{1 + a_1 z^{-1} + \dots + a_n z^{-n}} \right) \left(\frac{b_0 + b_1 z^{-1} + \dots + b_m z^{-m}}{1} \right) \quad (5.14)$$

and renaming them as:

$$H(z) = H_{ar}(z)H_{ma}(z) \quad (5.15)$$

where $H_{ma}(z)$ is the moving average part and $H_{ar}(z)$ is the autoregressive part. These can then be written as substitution variables $V(z)$ (output from moving average system) and $Y(z)$ (output from autoregressive system), with the following substitution [10]:

$$V(z) = H_{ma}(z)X(z) \quad (5.16)$$

$$Y(z) = H_{ar}(z)V(z) \quad (5.17)$$

where $X(z)$ is the input signal and $Y(z)$ is the output signal. Then taking the inverse z-transform we can go back to the time domain realization and get the following pair of difference equations [10].

$$v(k) = \sum_{i=0}^n b_i x(k-i) \quad (5.18)$$

$$y(k) = v(k) - \sum_{i=1}^n a_i y(k-i) \quad (5.19)$$

From this we can see that we can obtain the filter coefficients directly from the transfer function, thus a direct representation and thereof its name "Direct Form I".

5.2.2 Direct Form II

"Direct Form II" is almost the same as "Direct Form I" but with a small change that gives it an advantage. This alternative form of the direct realization is obtained by just rearranging the auto-regressive part with a moving average part in 5.14.

$$H(z) = \left(\frac{b_0 + b_1 z^{-1} + \dots + b_m z^{-m}}{1} \right) \left(\frac{1}{1 + a_1 z^{-1} + \dots + a_n z^{-n}} \right) \quad (5.20)$$

thus

$$H(z) = H_{ma}(z)H_{ar}(z) \quad (5.21)$$

Then the interchange affects the substitution variables as follows:

$$V(z) = H_{ar}(z)X(z) \quad (5.22)$$

$$Y(z) = H_{ma}(z)V(z) \quad (5.23)$$

which gives the following time domain representation

$$v(k) = x(k) - \sum_{i=1}^n a_i x(k-i) \quad (5.24)$$

$$y(k) = \sum_{i=0}^n b_i v(k-i) \quad (5.25)$$

By comparing the flow graphs of these two different realizations it can be seen that the Direct Form II has the advantage of taking up less computing memory than Direct Form I for the delay elements. This is also usually called the canonic representation.

Table 5.1: Number of required storage elements

Realization type	Number of storage elements (N)
Direct Form I	2N
Direct Form II	N

5.3 Filter Stability

We can write the transfer function of a IIR digital filter as a ratio of two polynomials of the z -transform as shown before in section 5.13, with the zeros $B(z)$ and poles $A(z)$ and thus form the following transfer function:

$$H(z) = \frac{B(z)}{A(z)} \quad (5.26)$$

where $A(z)$ is the polynomial in the denominator containing the filter poles.

$$A(z) = 1 + a_1z^{-1} + \dots + a_nz^{-n} \quad (5.27)$$

From the theory of continuous-time-systems we know that for stable filters all the poles have to lie in the left half part of the $Re\{z\}$. In order to apply this to digital filters we have first to map the poles into the z -plane and in order to get a stable filter all the poles have to lie inside the unit circle. This gives a constriction on the possible values that the poles can have, the criteria being that they can not have a magnitude larger than one.

Thus for a stable system the following condition has to be met

$$|a_k| \leq 1 \quad (1 < k < n) \quad (5.28)$$

6 Variance Propagation and Reduction Models

The agreement of consecutively daily time series depends strongly on the correlation between them. So in this section we will derive a model for the propagation of variance in the sidereal filter and the reduction in RMS, called Γ . We will then extend this model to the reduced sidereal filter by modeling and adding a scaling factor to the sidereal filter.

6.1 Sidereal Filter Model

To compute how the variance (or standard deviation) changes when sidereal filtering is applied, we first begin with setting up the sidereal filtering equation.

$$X_1^F = X_1 - \frac{1}{2}(X_1 + X_2) \quad (6.1)$$

where X_1 and X_2 are two random variables describing the time series for two consecutive days. Then by taking the expected value of the SDF equation we can set up an expression for the variance of the two variables [9].

$$E[(X_1^F)^2] = E[(X_1 - \frac{1}{2}(X_1 + X_2))^2] \quad (6.2)$$

To find the expression for the variance we compute the covariance of the two independent variables scaled by their standard deviation, by using 3.7 and 3.8.

$$Cov(X_1, X_1) = \sigma_1^2 \quad (6.3)$$

$$Cov(X_1, X_2) = \sigma_1 \sigma_2 \rho \quad (6.4)$$

$$Cov(X_2, X_2) = \sigma_2^2 \quad (6.5)$$

By substituting these 6.2, we can formulate the following variance model for the sidereal filter.

$$\sigma_F^2 = \frac{1}{4}(\sigma_1^2 - 2\sigma_1\sigma_2\rho + \sigma_2^2) \quad (6.6)$$

where σ_F^2 is the variance after filtering is applied, σ_1^2 and σ_2^2 is the different variance from day 1 and day 2, and ρ is the correlation coefficient between day 1 and day 2. To simplify this expression we use the assumption that the variance from day to day is approximately equal by letting $\sigma_1 = \sigma_2 = \sigma_X$, then the expression for the model becomes:

$$\sigma_F^2 = \frac{1}{2}\sigma_X^2(1 - \rho) \quad (6.7)$$

We now have a model to describe the propagation of variance in the filtered time series, we will now define the root-mean-square ratio to model the reduction in RMS when sidereal filtering is applied. This is done by defining a expression for the reduction in RMS as followed,

$$\Gamma_{sdf} \equiv \frac{\sigma_F}{\sigma_X} \equiv \sqrt{\frac{1}{2}(1 - \rho)} \quad (6.8)$$

where Γ is the ratio between the original RMS and the filtered RMS. By combining Eq6.7 and 6.8 we get the following model for the reduction in RMS in percent.

$$\Gamma_{sdf} = 100 \cdot \left(1 - \frac{\sigma_F}{\sigma_X}\right) = 100 \cdot \left(1 - \sqrt{\frac{1}{2}(1 - \rho)}\right) \quad (6.9)$$

Worth noting is that the model only depends on one input parameter, the correlation between the two variables X_1 and X_2 . Thus the reduction of RMS is only a function of the correlation coefficient.

6.2 Reduced Sidereal Filter Model

To be able to model the reduction of RMS (or variance) in the reduced sidereal filter we extend the SDF-model by making the following model assumption. The reduction in RMS (or variance) is proportional to the signal amplitude.

$$\sigma^2 \propto A_{signal} \quad (6.10)$$

This assumption comes from that the variance in the time-domain must be dependent on the signal amplitude and thus also to the signal power from the in the frequency domain. Assuming a deterministic sinusoidal periodic signal, we can write the amplitude as a function of signal power:

$$A = \sqrt{2P} \quad (6.11)$$

Solving for the amplitude we can find a expression to define a scaling factor to be used to model the reduction of RMS in the RSDF by extending the SDF-model by multiplying it with α .

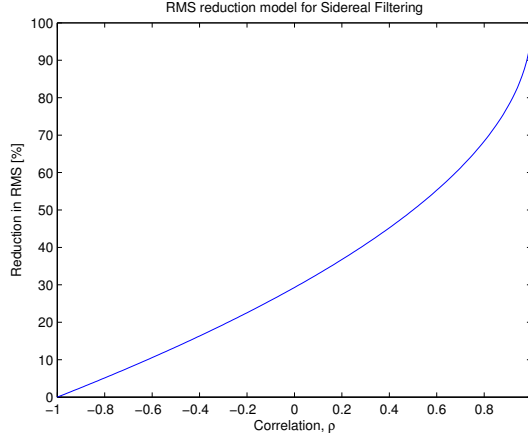


Figure 6.1: Showing the modeled reduction in RMS, Γ_{sdf} , as function of the inherent correlation, ρ , between the time-series of the sidereal filter design days, described by Eq. 6.9

$$\Gamma_{rsdf} \equiv \alpha \cdot \Gamma_{sdf} \quad (6.12)$$

By using the relations described in Eq. 6.11 and the peak to peak amplitude, we can define α as follows:

$$\alpha \equiv 2\sqrt{2P_{signal}} \quad (6.13)$$

This can be understood in the following way: we know that removing power from the time series will affect the variance (from Parseval's theorem). Thus the power in the RSDF approach and the SDF approach can be expressed as follows:

$$P_{rsdf}^F = P_{tot} - P_{signal} \quad (6.14)$$

$$P_{sdf}^F = P_{tot} \quad (6.15)$$

where P_{filter}^F describes the total power contained in the two different filter. By definition the RSDF always has to contain less power than the SDF.

$$(P_{rsdf}^F < P_{sdf}^F) \quad (6.16)$$

By applying the two different filters to the time series the following power relations are obtained.

$$P_{rsdf} = P_{tot} - P_{rsdf}^F \quad (6.17)$$

$$P_{sdf} = P_{tot} - P_{sdf}^F \quad (6.18)$$

From this we then finally note that the power in the RSDF filtered time series is always larger than in the SDF approach, thus the reduction in RMS is always smaller in RSDF than in the SDF case.

$$(P_{rsdf} > P_{sdf}) \rightarrow (\Gamma_{rsdf} < \Gamma_{sdf}) \quad (6.19)$$

From this it can be seen that to model the RSDF we not only have to know one parameter (ρ) we also have to have knowledge about the power/amplitude in the signal band. To model the reduced sidereal filter we need to know both α and ρ , then the reduction in RMS for the RSDF is a function of two parameters $\Gamma_{rsdf}(\alpha, \rho)$.

7 GRASP Software Description

GRASP is abbreviation for "GPS Residual Analysis Program" and is a graphical user interface (GUI) program developed in MATLAB for GPS data editing, by Johan Nilsson. GRASP is a program for visual editing of GPS carrier-phase position estimate residuals from the program BAKAR.

BAKAR is a program for GPS kinematic relative positioning (described in 2.9) of single-frequency carrier-phase GPS data. It uses the double difference technique (described in 2.5) to process single baseline data position estimate data. The program requires two RINEX files for each day of data, GPS orbit information and the program also assumes that the stations are close by to cancel out ionospheric and other baseline related effects (see section 2.6). BAKAR was developed by James L. Davis and Pedro Elosegui.

GRASP is developed to visually detect and remove outliers and cycle slips in the double differenced residuals (estimated from the mean site position). These edited data points are then saved into a log file and marked with their corresponding timeepochs. This log file is then used as input to BAKAR for re-processing of the raw observed position where the marked epochs in the log file are corrected for in the raw data. This will then give a more accurate solution and this procedure is repeated until satisfactory residuals are obtained.

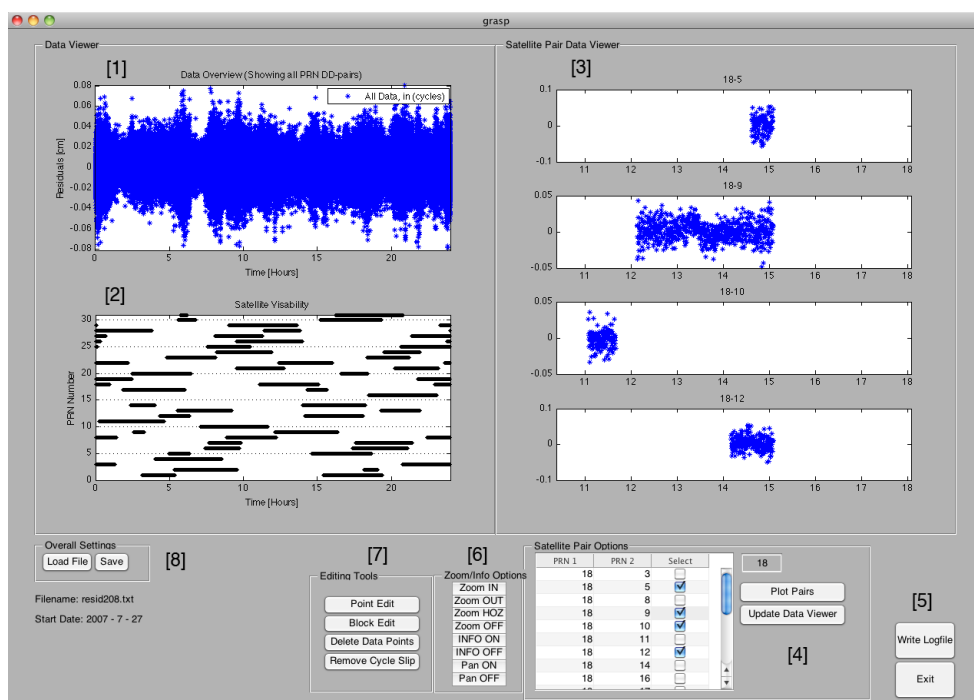
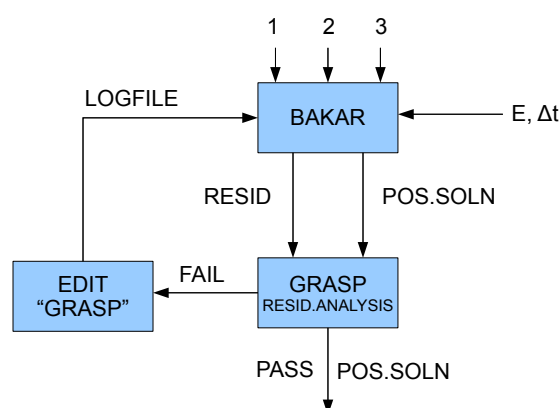


Figure 7.1: Showing desktop layout of GRASP software and indicators (1 - 8) of different GRASP visualization windows and tools/functions

Table 7.1: Function description for GRASP

Number	Description
1 :	Shows all available residuals of the different PRN DD-pairs.
2 :	Shows available data overlap for different epochs in loaded batch.
3 :	Dynamic plot of chosen PRN-pairs (reference satellite concept).
4 :	Adding PRN-reference. Select PRN-Pairs. Plot selected pairs in (3). Update Data Viewer: Updates (1) after changes are made in (3).
5 :	<u>Write Logfile</u> : Writes a log of edited epochs (done last!). <u>Exit</u> : Exit program.
6 :	Available Zoom and Info options that can be applied to data.
7 :	<u>Point Edit</u> : Editing single data point. <u>Block Edit</u> : Editing multiple points. <u>Delete Data Points</u> : Deletes the selected data points. <u>Remove Cycle Slip</u> : Indicate and remove cycle slips, with specific integer.
8 :	<u>Load File</u> : Select and load residual data file. <u>Save</u> : Saves changed data as .txt file to be opened again for further editing.



1. RINEX files
 2. Clock/Orbit files
 3. Site position file

E = Elevation cutoff
 Δt = Sampling time

pos.soln = Position Estimates
 resid = Residuals

Figure 7.2: Flowchart for the processing strategy of the BAKAR–GRASP data processing.

RINEX is short for (Receiver Independent Exchange Format) and is a interchangeable format for raw satellite navigation data which allows the user to perform off-line post processing to produce an improved position solution. The format stores the observables of pseudo-range and carrier-phase measurements, described in section 2.3. For BAKAR two RINEX files is needed to calculate the baseline between two stations (one for each station).

Clock and Orbit files are the improved estimates of the satellites orbit and clock solution, this makes it possible in the post-processing to remove, by the differencing techniques (described in section 2) errors due to clocks and orbit. Which greatly improves position accuracy. The site position file contains previously known locations for the receiver. This helps to speed up the processing scheme by less iterations to estimate a new accurate position.

The elevation cut-off angle is important due to the fact that observations at low elevations angles are more affected by the atmosphere (mostly troposphere, see 2.6.6). So by excluding observations lower than a specific elevation will help to reduce the level of noise in the position estimates. Usually an angle between 10–20 degrees is considered to be the rule of thumb for GPS data processing.

The sampling time of the RINEX file determines the temporal resolution.

8 Data Processing and Methodology

In this section the data processing strategy and the methodology used will be presented. The goal is to estimate the unknown parameters and to determine optimum implementation techniques for the different filtering approaches.

8.1 Processing Strategy

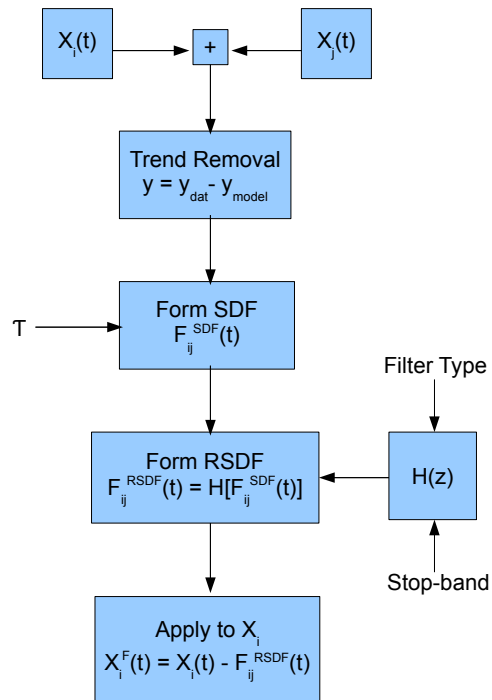
We will introduce the processing strategy used to construct the reduced sidereal filter and show the major different steps in the process.

To construct the sidereal filter one needs a minimum of two consecutive days of data (X_i and X_j) which are merged into a common time series.

This time series has then to be de-trended to be able to evaluate the geodetic signals and noise inherent within the data structure. Then the sidereal filter can be found by identifying and averaging the corresponding epochs shifted by the sidereal time shift τ .

To be able to detect and evaluate the periodic signals, when using the sidereal filtering approach a digital filter has to be applied to the SDF-filter. This by identifying the signal and noise band and then choosing a digital filter which fulfills the desired spectral specifications.

Finally when the RSDF filter is constructed (after applying a digital filter to the SDF) we apply it to the original time series, using time domain filtering. This will preserve the periodic or common mode behavior in the data. Ordinarily filtered away by the SDF-filter.



T : Sidereal time shift.
 Stop-band : Frequency range to remove.
 Filter Type : What type of digital filter to use.
 H(z) : Digital Filter.
 i : Day number.
 j : j= i +1 .

Figure 8.1: Flowchart for the processing strategy for reduced sidereal filter implementation.

8.2 Implementation & Parameter Estimation of Sidereal Filter

The sidereal filter foundation lies in the agreement of the day to day time series from which the filter is constructed from. Where the agreement is measured by the correlation. To construct the filter we use two consecutive days and a sidereal time shift based from 15 s sampling time. The time shift used was 23h 56m 00s (ordinary sidereal repeat time 23h 56h 04s).The sidereal time shift was cut to fit the sampling time.

Next we find the optimum way to construct and implement the sidereal filter. There are two methods to do this. In the first method we define the static filter approach. Where the filter is built from day one and two F_{12} . Then this filter is applied to the rest of the time series $X_i^F = X_i - F_{12}$. The second method we define as the moving filter approach. Where the filter is re-built when moving through the time series and applied only on the day which they are constructed for as follows, F_{ij} where ($j = i + 1$) and applied as follows $X_i^F = X_i - F_{ij}$.

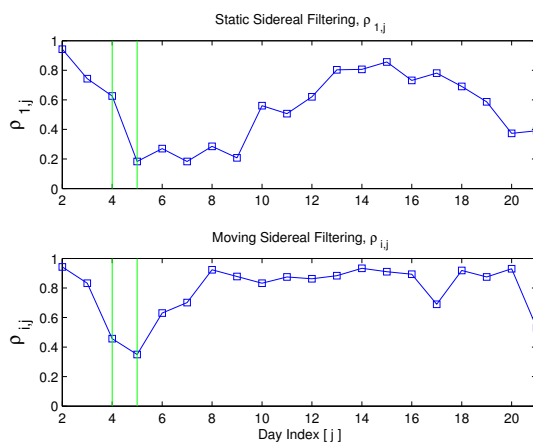


Figure 8.2: Showing the de-correlation of the time series of the static (top figure) and the moving (bottom figure) sidereal filtering. Green vertical lines indicates days where glacier earthquakes occurred. Further i is the day number and $j = i + 1$.

In order to obtain the best filter performance high agreement (i.e high correlation) is required. By investigating the correlation of the time-series for the different design and filter implementation we can find which of these that gives the highest average correlation.

From Figure 8.2 we find that the highest average correlation is achieved by the moving filter implementation approach (F_{ij} , from ρ_{ij}). Thus this is the filter implementation chosen for this thesis.

8.3 Implementation & Parameter Estimation of Digital Filter

To be able to apply our digital filter to the sidereal filter and form the reduced (extended) sidereal filter we have to define the signal and noise band. This is done by investigating the spectral content of the sidereal filter and locate the signal components.

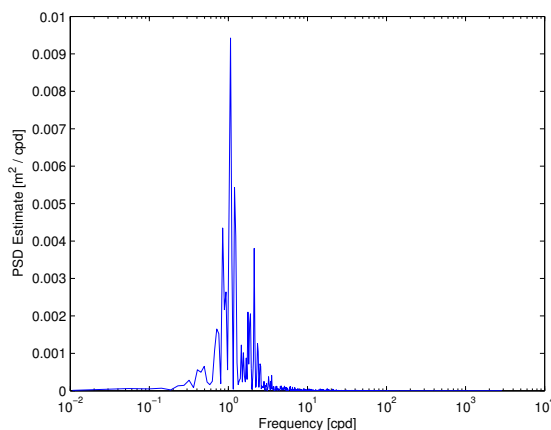


Figure 8.3: Periodogram of high resolution ($\delta_f = 0.05$ cpd) PSD-estimate of de-trended along track glacier flow. Where the tidal band lies between 0.35 – 3 cpd.

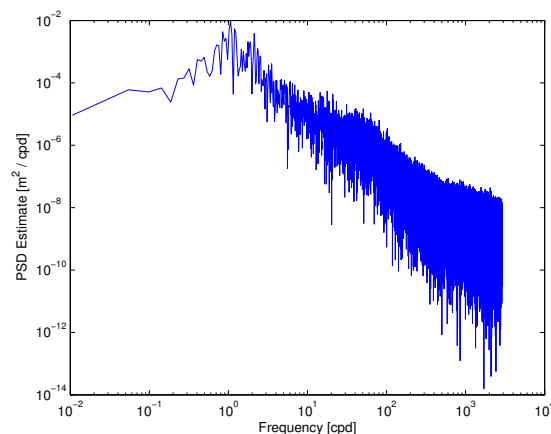


Figure 8.4: Periodogram of high resolution ($\delta_f = 0.05$ cpd) PSD-estimate, in logarithmic scale, of de-trended along track glacier flow. Where the tidal band lies between 0.35 – 3 cpd.

From Figure 8.3 and 8.4 we can see that the signal band is located in the range of 0.35 – 3 cpd which contains most of the power, see Figure 8.5. In this thesis we consider all spectral components outside this band as noise.

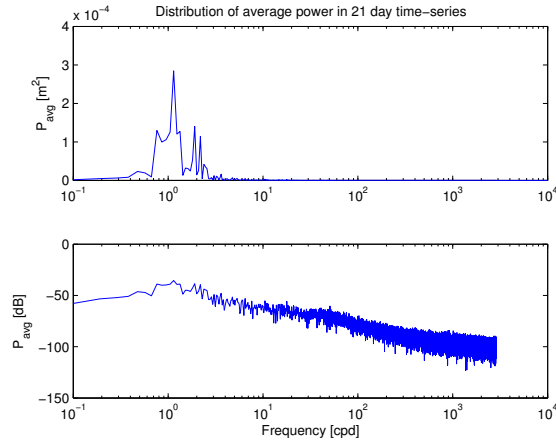


Figure 8.5: Distribution of integrated average power in the original time series of 21 days. With a frequency resolution of $\delta_f = 0.01$ cpd.

Then a trial and error approach was used to determine the optimum digital filter type and parameters. Since the tidal band is in the low frequency range (1 – 3 cpd) these frequencies lies in the first 10 – 20 samples. In this sample range the filter transient play a large roll when choosing the filter order and the type of filter. We do not want to introduce a transient behavior, such as ghost signals or over estimation of the signal (due to signal amplification from transient responses). To overcome this four cascaded notch filters was used centered around $F_c = 1, 2, 2.5$ and 3 cpd, with corresponding bandwidths of 13, 8, 3 and 1 cpd and a filter order of $N = 2$.

The notch filter was chosen due to that the bandstop filter with $N > 2$ introduced transient behavior. And $N = 2$ did not give a sharp enough roll off to remove signal band frequency components without affecting adjacent frequencies at an unacceptable level.

The constructed digital filter gave the following filter frequency magnitude response.

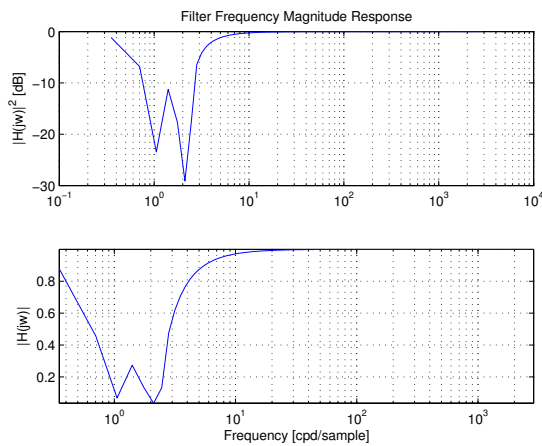


Figure 8.6: Digital notch filter frequency response, in the form of magnitude

Further the phase and group delay response for the digital filter.

From Figure 8.6 we can see that the specification in the filter frequency response to filter out the signal band in the sidereal filter have been fulfilled to a satisfactory extent. There is some reduction in adjacent frequencies up to around 10 cpd, but the reduction is minor and can be accepted. The phase and group delay of the filter is of minor interest

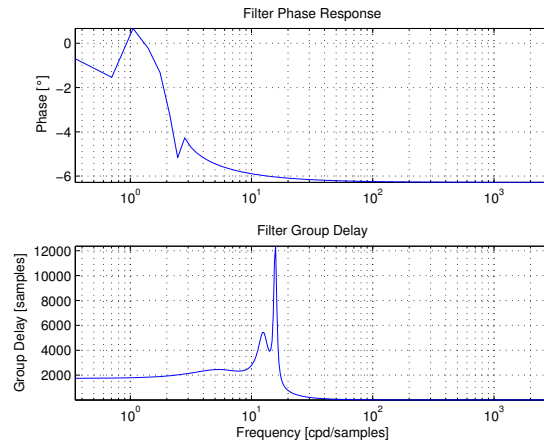


Figure 8.7: Digital notch filter frequency response, in the form of phase and group delay

due to the fact we take the absolute value squared when computing the power spectral density, the effect of the group delay seems to be small.

Finally we need to investigate if our digital filter is stable, by plotting its poles and zeros.

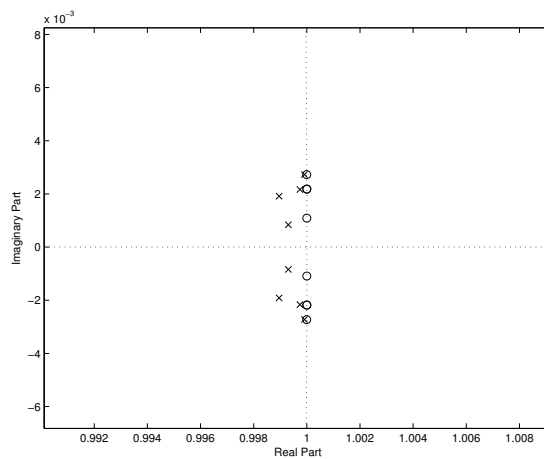


Figure 8.8: Showing poles and zeros of digital filter to determine filter stability using the unit circle.

From Figure 8.8 we can determine that the filter is stable due to the fact that all the poles are inside the unit circle.

9 Results

The processing of the 21 day time series gave 20 days filtered time-series after the reduced and ordinary sidereal filtering was applied to the data set. With the processing parameters described in Section 8.

For the IS22 station, a station velocity of 19.7 m/day was observed before the detected glacial earthquake on day 4 (189) and 5 (190) and an observed station velocity of 22.8 m/day after the glacial earthquake.

9.1 Filter Performance

From Figure 9.1 we see an improvement in in the time series filtered with the RSDF-filter in the form of a decrease in higher frequency noise and that the periodic signal dynamics are largely preserved. For the SDF-filtered time series we see a high reduction in variability (i.e periodic signals) and a large reduction in higher frequency noise. Further observed in the SDF filtered time series is an increase in amplitude (transient signal), starting on day 2 (187), which seems to corresponds the rapid change in glacier surface area, observed by [5]. This transient signal can be identified both in the original and the RSDF-filtered data set, but they are more hidden behind periodic signals.

The observed standard deviation (RMS) for the original, RSDF and SDF are 43.5 mm, 39 mm and 17 mm. Which corresponds to a reduction in variability of 10% and 61% respectively compared to the original standard deviation.

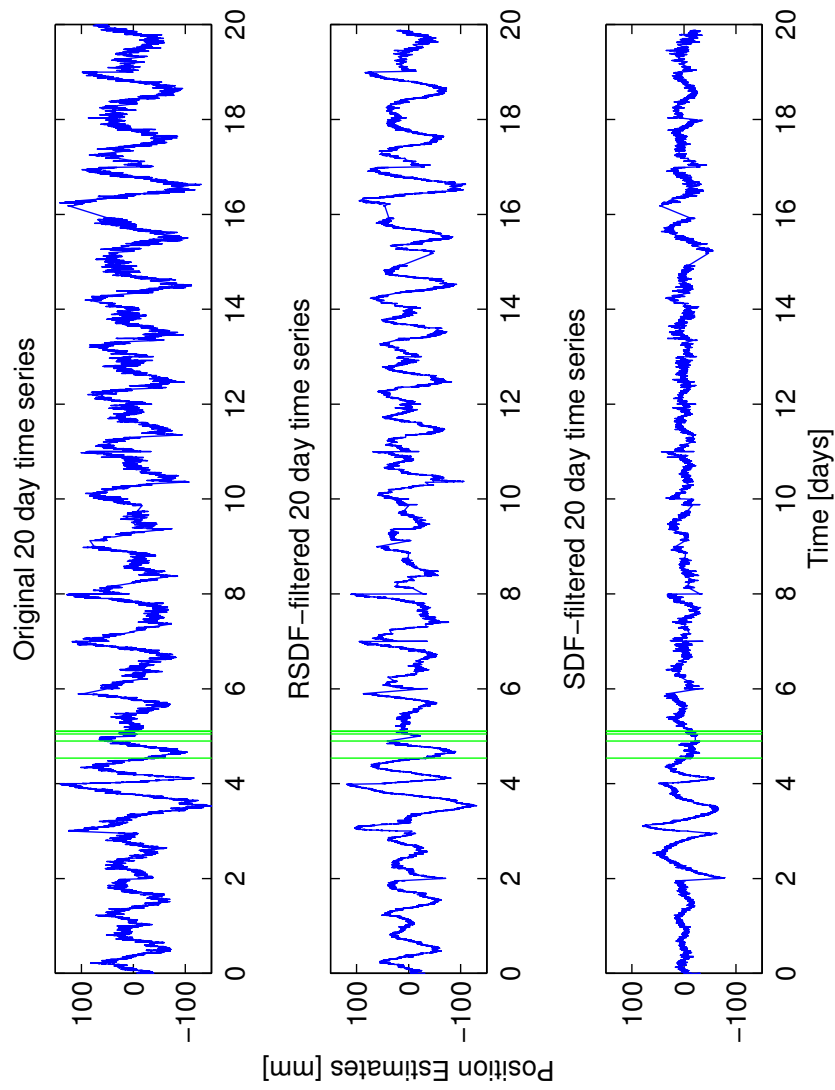


Figure 9.1: De-trended 20 day time series of position estimates for the RSDF-filtered, the SDF-filtered, and the original time series. Green vertical lines indicate glacial earthquakes.

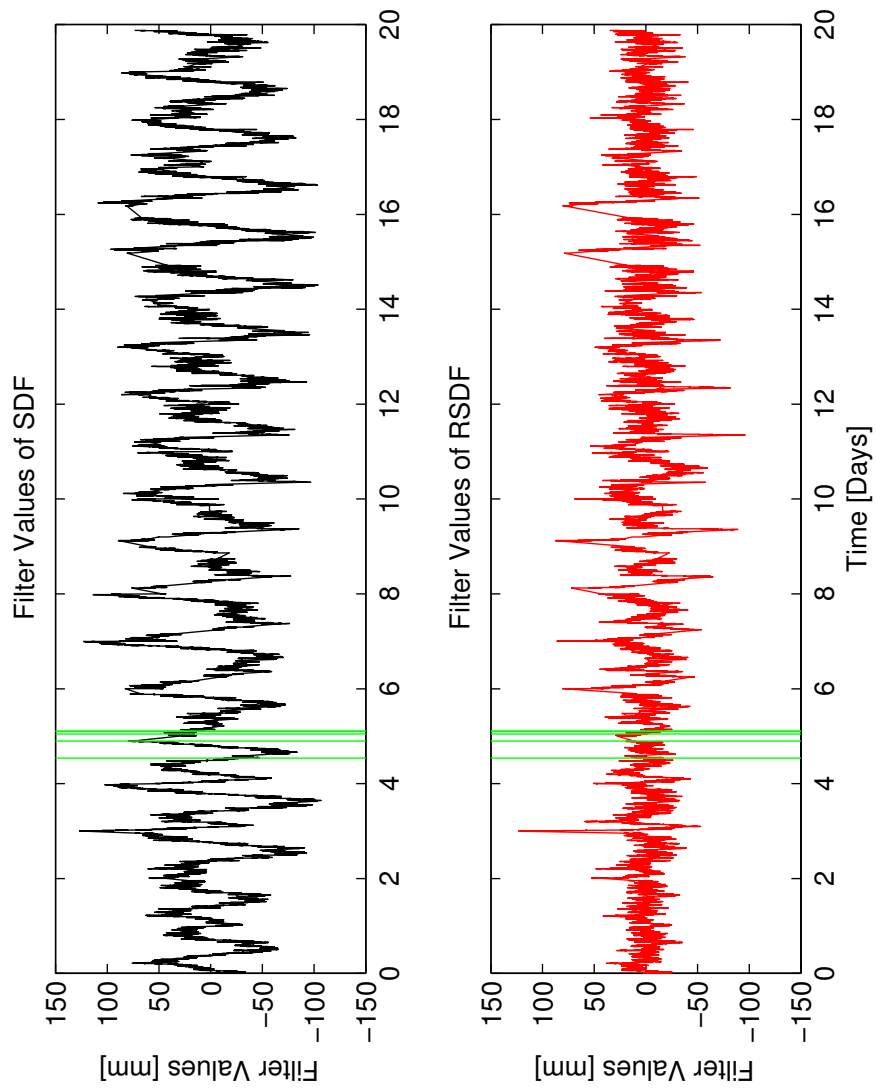


Figure 9.2: Filter values for the 20 day time series for the RSDF and SDF filter. Green vertical lines indicate glacial earthquakes epochs.

In Figure 9.2 we observe that the filter values for the SDF-filter closely resembles the original time series with the periodic variations mostly caused by diurnal and semi-diurnal tidal signals, located at 1 and 2 cpd in Figure 8.3 (which are the dominant periodic signals in the defined signal band). For the RSDF-filter we observe that the notch filters (digital filter implementation) have largely succeeded in removing the signal band from the filter values (periodic signals including diurnal and semi-diurnal components). Left in the filter values is mostly noise (predominantly multipath, due to GPS data processing), with some lingering period behavior that the digital filter was not able to remove. They are located between day 6 – 9 and day 15 – 16 and are mostly tidal signal components. The following standard deviations observed for SDF was 39.5 mm and for RSDF 16.8 mm, which gives a decrease in variability with a factor of 2.35.

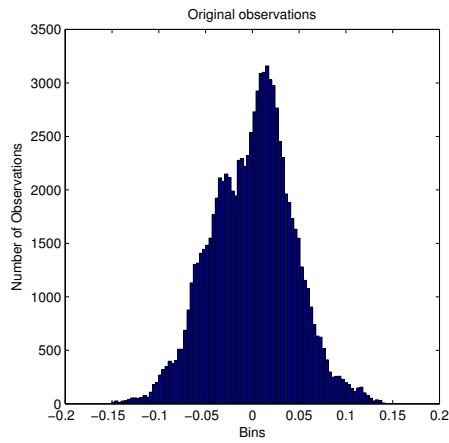


Figure 9.3: Histograms of the original 20 day time series.

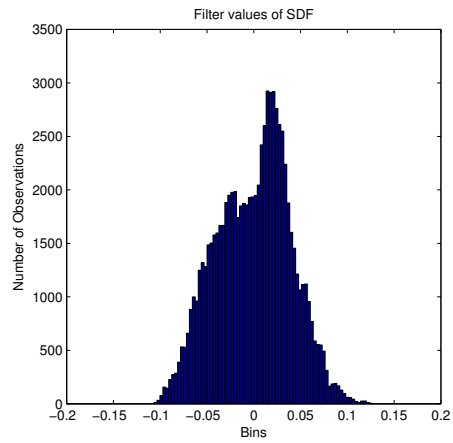


Figure 9.6: Histogram of the filter values of the SDF-filter.

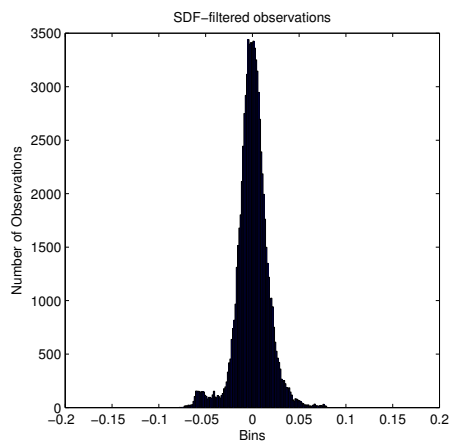


Figure 9.4: Histogram of observations filtered with the SDF approach.

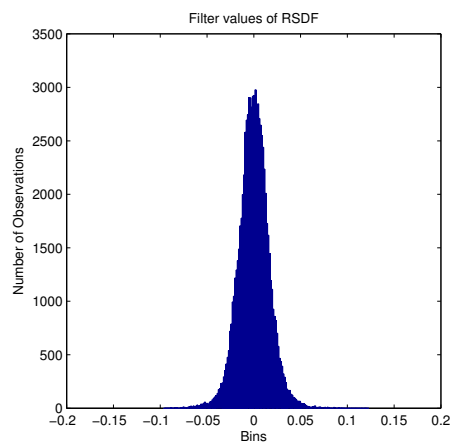


Figure 9.7: Histogram of the filter values of the RSDF-filter.

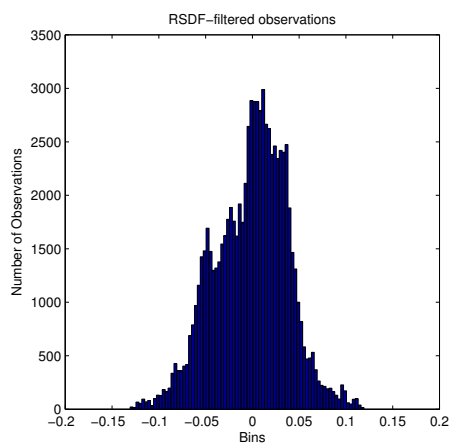


Figure 9.5: Histogram of observations filtered with the RSDF approach.

Figures 9.3, 9.5 and 9.4 show the histograms of the filtered time-series compared to the original. We observe that the SDF shows the largest change, where the width and flanks of the distribution (largely gaussian) have clearly been reduced compared the original data set. This indicating a reduction in both the variability and in the noise. In the RSDF histogram we observe that the overall shape of the distribution is kept intact. However the flanks of the sides have been retracted and the slope of the sides (vertically) of the distribution is now sharper and the width (of the shape) is smaller. This points to a noise reduction and a approximately equal variability from before and after RSDF filtering.

Figure 9.6 shows the filter values form the SDF filter and observed here is that the overall shape of the distribution is preserved compared to Figure 9.3. But the absence of the tails indicates a reduction i noise, due to a smoothing effect when constructing the filter from averaging. In Figure 9.7 which shows the filter values from the RSDF filter we observe a clear gaussian distribution. Corresponding to gaussian white noise. This due to removal of the all signals in the signal band leaving mostly (multipath) noise.

We can observe that both the filtered RMS, the signal and the noise power characteristics varies with the moving correlation for the different days, seen in figures ?? – ??. A drop in the correlation is consistent with an increase in the filtered RMS and an increase of both the noise and the signal power (applies to both the SDF and the RSDF results).

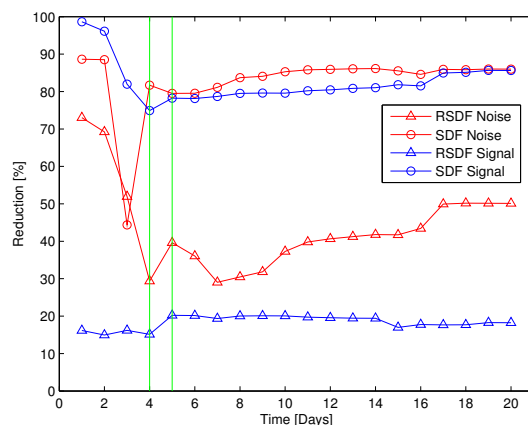


Figure 9.8: Signal degradation and noise reduction for the reduced and ordinary sidereal filter. Green vertical line indicates days with glacial earthquakes.

In Figure 9.8 we see a sharp drop in noise reduction for the SDF and RSDF filter, starting at day 2 (187). For the SDF filter the decrease in noise reduction is consistent with the rapid change in glacier surface area, noticed in [5], pre-dating the earthquake epoch with one day. The decrease in noise reduction observed in the RSDF filtered data is also consistent with the change in glacier surface area, but also with a sharp increase in station velocity at day 4 (189), also seen in [5]. Investigating the noise reduction curve for the RSDF-filtered data we observe a increasing trend in noise reduction, approximately $\sim 1.6\%$ per day. This increase seem consistent with the stations velocity profile, from day epoch 2 – 20 (189 – 205), observed by [5].

The median and standard deviation of noise reduction and signal degradation is summarized in Table 9.1.

Table 9.1: Summary of signal degradation and noise power reduction statistics

χ	Band	$\tilde{\mu}_x$ [%]	σ [%]	min [%]	max [%]
RSDF	Noise	41.5	12	29	73
	Signal	19.0	1.7	15	20
SDF	Noise	86.0	9.4	44	89
	Signal	81.0	1.7	75	99

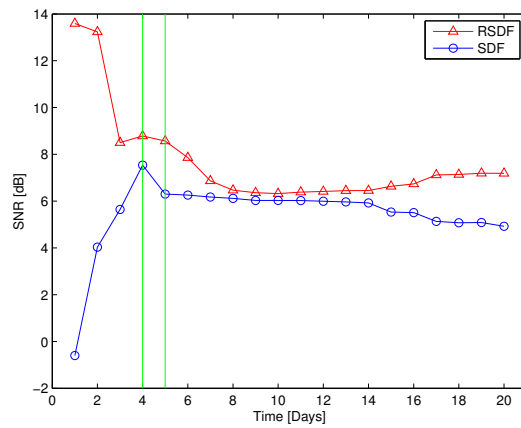


Figure 9.9: Signal to noise ratio (SNR) for the reduced and ordinary sidereal filter. Green vertical lines indicate days glacial earthquakes.

The SNR observed in Figure 9.9 shows that the signal to noise ratio is considerably higher for the RSDF filtered data than the SDF-filtered data.

Table 9.2: Summary of SNR statistics

SNR	μ_x [dB]	σ [dB]	min [dB]	max [dB]
RSDF	7.7	2.1	7	14
SDF	5.4	1.6	2	6.5

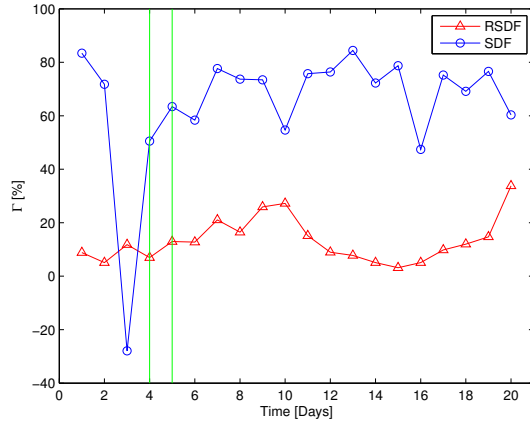


Figure 9.10: Reduction of RMS for the RSDF and the SDF approach. Green vertical lines indicates days with glacial earthquake.

In Figure 9.10 we observe that the reduction in Γ_{sdf} have a close relationship to the change in correlation of the time series. With a significant drop in Γ_{sdf} pre-dating the glacial earthquake epoch with one day, consistent with a rapid reduction of glacier surface area. Γ_{rsdf} reduction in RMS follows the original RMS (then also correlation) of the data set and where the change in surface area is not noticed. The observed reduction in RMS in 9.10 is consistently smaller in the RSDF than the SDF approach, consistent with the removed power from the RSDF filter, described in theory.

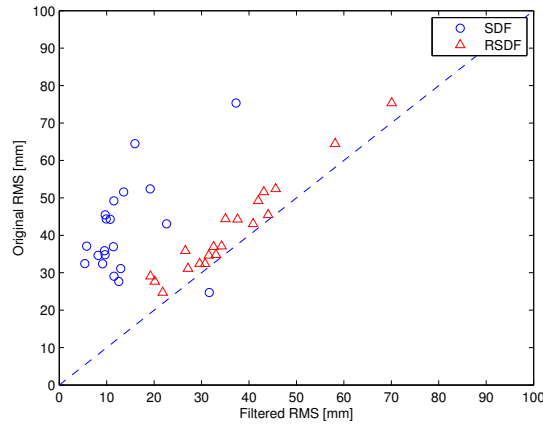


Figure 9.11: Deviations in the filter performance for the processed data for the RSDF and the SDF approach.

Table 9.3: Summary of RMS reduction statistics for RSDF and SDF

Γ_{rms} [%]	$\tilde{\mu}_x$ [%]	σ [%]	min [%]	max [%]
RSDF	12	8.2	3.2	34
SDF	73	24	-28	84.5

9.2 Validation of Model

Figure 9.12 depicts the agreement between observed and modeled reduction of 99.0 % for the SDF-model, And an agreement for the RSDF-model of 81%. With the corresponding standard deviations of 0.63 % and 0.97 % receptively (agreement determined using median reduction).

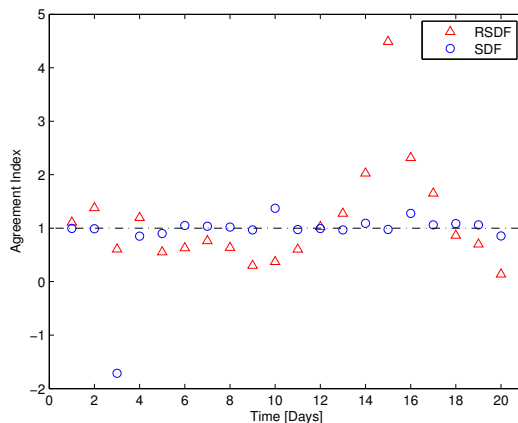


Figure 9.12: Agreement between RMS-models and observed data for Γ . The agreement index is defined as: $(\Gamma_{model}/\Gamma_{data})$.

Figure 9.13 depicts model deviations. With some values that lies outside of the norm and can be considered outliers for both the SDF and RSDF model compared to real observations. Other values larger deviations would be consistent with de-correlation.

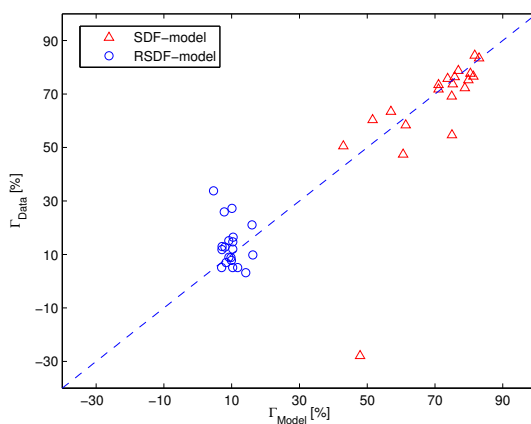


Figure 9.13: Deviations of observed reductions in RMS compared to the modeled reductions in RMS.

From Figure 9.12 and 9.13 we observe that the developed models for the reduction in RMS fit the observed values well. This indicates that the correlation of the time series well describes the dynamics of sidereal filter. Further including the signal amplitude into the reduced sidereal filtering model gives adequate agreement to describe the filter dynamics.

10 Discussion

In general the correlation of the time series seems to give a good description of agreement of the day to day behavior of the time series. And to also characterize the filter performance. Due to the fact that correlation is only a description of the linear dependence of two variables it does not give a full description of the different dynamics affecting filtering performance. We have seen that roughly rapid (linear) behaviors can be seen in the correlation such as the change of surface area (see [5]). However, it does not seem to encompass the change in station velocity (velocity profile, see [5]) to a full extent (only rapid linear changes). This means that we also have to take into account the station station velocity profile when determining filter capability for the reduction of noise. The degradation of signal for the RSDF and SDF filtering approach on the other hand seems stable for both the SDF and the RSDF. This is likely due to that they are highly correlated in time. Why there is a large difference in noise reduction for the two approaches (they are very alike) is not yet understood and need to be investigated further. There might be a string of contributions to this, such a induced effect due to the application of the digital filter, inherent signal and noise structures or other factors. Longer time-series, to see if this pattern is consistent, would be of great interest to further investigate this phenomena.

The hypothesis regarding what governs the performance of noise reduction (ΔA and Δv) is that the change in glacier surface area is proportional to the multipath reflective area (number of reflection points) which means that a rapid change in surface area will change the total number of reflected multipath signals (power), thus de-correlating the noise in the time-series over time. This can be seen in 9.1 for the SDF filter on day 3 (188), where a sharp drop in noise reduction is observed to happen at the same epoch as a sharp drop in glacier surface area, see [5], once the area stabilizes, noise reduction returns to previous levels, see [5]. Further can be argued that the change in station velocity or it's profile is connected to the surface topology (roughness). Where the change in surface topology will change the distribution of multipath power (spread it in space), this assuming constant glacier surface area. This means that the velocity profile (station acceleration) rapidly takes the station through different surface structures over time, changing reflective power distributions and thus de-correlating the received noise in the time-series over time.

The models developed for the thesis have been built to find and characterize the reduction in variability and thus also understand the underlying governing dynamics controlling filter performance. The developed models which uses the correlation and amplitude as governing factors shows good agreement with observed reduction in variability, even with the simple model assumptions made ($\sigma_1 = \sigma_2$ and $A = 2\sqrt{2P}$). From the model and data agreement we can clearly state that the correlation of the time series is the main factor controlling the dynamics (easiest seen in the SDF), but also on the maximum signal strength (RSDF). The reduction in variability does not give the full insight into the reduction in noise. Mostly only to the reduction of the common-mode and periodic signals. Still by using the fact that if we know the correlation of the data set we also know to some extent the correlation of noise. This means that you will get a indirect insight into noise reduction when you measure the reduction in variability (degradation of signal). Measuring the reduction in variability can be the first step to see if the sidereal filtering approach is applicable to the specific data set and the general filtering performance.

The SNR measured for the two different approaches give us insight that the RSDF approach has a much better result in preserving the dynamics of the signals in the data set, whilst still giving a good noise reduction capabilities. The SDF approach on the other hand have a larger/better noise reduction capabilities but with the tradeoff that common mode signals are also removed. But for the SDF case we can also argue that this is a good

trait if we are interested in only transient signals. Which for the RSDF is harder to see due to that they are usually hidden in the other periodic signals.

11 Conclusion

We have found that its possible to extend the sidereal filtering technique to a highly dynamic and kinetic environment such as the Helheim glacier. It is further possible to extend sidereal filtering to encompass the evaluation of periodic signals in general in this environment. Doing so with a high level of reduction in multipath noise and acceptable geodetic signal degradation (for RSDF only).

By investigating the SNR of the for the different filtering approaches we found that the RSDF approach consistently gave a higher signal to noise ratio than the ordinary sidereal filtering which makes it overall a better instrument to investigate geodetic signals. The SDF approach is however better at evaluating transient signals and still has higher noise reduction capabilities than the RSDF approach, with the trade-off that it does not encompass periodic behavior.

We further conclude that the reduced sidereal filtering is sensitive, especially the noise reduction, to the station velocity profile and change in the glacier surface area (its reflective properties). While the ordinary sidereal filtering seems to only be affected by the change in glacier surface area.

We also found that the correlation of the time series is a good measure of the agreement of the day to day time series and well describes the filter performance. However it does not give full insight into the noise and signal dynamics in the data (due to the fact that its a measure of linearity). It encompasses changes in glacier surface area but not the station velocity profile.

12 Future Work

Future work for this thesis would be to improve the implementation of the digital filter. The current processing strategy has a draw back. This draw back is that the frequency resolution in the data is to low in the current processing strategy. The implication being that the frequency components of interest is contained in the first samples of the data set. This region is heavily affected by the filter transient and the digital filter and its filter order has to be chosen properly to be able to handle this. This makes it difficult to get the desired effect from the filter without affecting the data in a negative way.

A solution to this problem would be to reverse the processing strategy accordingly:

1. Merge the day to day time series into one N -day time series.
2. Construct sidereal filter using N -day time series. Filter length is then: $F_{N-1} = X_N - 1$.
3. Apply digital filter to F_{N-1} (improved frequency resolution).
4. Cut X_{N-1} into daily time series and perform signal and noise analysis.

Another strategy would be to apply zero padding (adding N zeros) to the time series. Then apply the digital filter to the zero padded time series.

These two strategies would increase the frequency resolution of the data set ($\delta_f = 1/T$) when the digital filter is applied. Pushing the relevant frequency information out of the filter transient region. Thus making it possible to use higher filter order and other possible digital filters.

References

- [1] H. Lichtenegger B. Hoffman-Wellenhof and J.Collins et al. *GPS Theory and Practice, fifth edition*. SpringerWienNewYork, 2000.
- [2] Dietrich Schlichthäle et al. *Digital Filter: Basics and Design*. Springer, 2000.
- [3] Geoffrey Blewitt et al. *Geodetic Applications of GPS, Basics of the GPS Technique: Observational Equations*. Swedish Land Survey, 1997.
- [4] Gunter Seeber et al. *Satellite Geodesy*. Walter de Gruyter.
- [5] Meredith Nettles et al. Step-wise changes in glacier flow speed coincide with calving and glacial earthquakes at helheim glacier, greenland. *J. Geophys. Res.*, 74, 2008.
- [6] Richard Shiav et al. *Introduction to Applied Statistical Signal Analysis: Guide to Biomedical and Electrical Engineering Applications, third edition*. Academic Press, Elsevier, 2007.
- [7] H. S. Hopefield. Two-quartic tropospheric refractivity profile for correcting satellite data. *J. Geophys. Res.*, 74:4487 – 4499, 1969.
- [8] D.E. MacNamara and R.I. Boaz. Seismic noise analysis system using power spectral density probability density function: A stand-alone software package. *U.S. Geological Survey, Open-File Report 2005-1438*, page 8, 2005.
- [9] J. Susan Milton and Jesse C. Arnold et al. *Introduction to Probability and Statistics: Principles and Applications for Engineering and the Computing Science, fourth edition*. McGraw Hill, 2003.
- [10] Robert J. Schilling and Sandra L. Harris et al. *Fundamentals of Digital Signal Processing: using MATLAB*. Thomson, 2005.
- [11] B.A Sheno. *Magnitude and Delay Approximations of 1D and 2D Digital Filters*. Springer, 1999.